Aurora B phosphorylates Bub1 to promote spindle assembly checkpoint signaling

Babhrubahan Roy[1], Simon J. Y. Han[1,2], Adrienne N. Fontan[1,3], Soubhagyalakshmi Jema[1], Ajit P. Joglekar[1,*]

1 – Cell & Developmental Biology, University of Michigan Medical School, Ann Arbor, MI, USA

2 – present address: University of Cincinnati College of Medicine, Cincinnati, USA

3 – present address: Massachusetts Institute of Technology, Cambridge, USA

* - corresponding author

Summary

Accurate chromosome segregation during cell division requires amphitelic chromosome attachment to the spindle apparatus. It is ensured by the combined activity of the Spindle Assembly Checkpoint (SAC) [1], a signaling mechanism that delays anaphase onset in response to unattached chromosomes, and an error correction mechanism that eliminates syntelic attachments [2]. The SAC becomes active when Mps1 kinase sequentially phosphorylates the kinetochore protein Spc105/KNL1 and the signaling proteins that Spc105/KNL1 recruits enabling the production of the Mitotic Checkpoint Complex (MCC) [3-8]. The error correction mechanism is regulated by the Aurora B kinase, but Aurora B also promotes SAC signaling via indirect mechanisms [9-12]. Here we present evidence that Aurora B kinase activity directly promotes MCC production by working downstream of Mps1 in budding yeast and human cells. Using the ectopic SAC activation (eSAC) system, we find that the conditional dimerization of Aurora B in budding yeast, and an Aurora B recruitment domain in HeLa cells, with either Bub1 or Mad1, but not the 'MELT' motifs in Spc105/KNL1, leads to ectopic MCC production and mitotic arrest [13-16]. Importantly, this requires the ability of Bub1 to recruit both Mad1 and Cdc20. These and other data show that Aurora B cooperates with Bub1 to promote MCC production, but only after Mps1 licenses Bub1 recruitment to the kinetochore. This direct involvement of Aurora B in SAC signaling likely enables SAC signaling to continue after Mps1 activity in the kinetochore is lowered.

Results & Discussion

A dissection of the contributions of Bub1 and Mad1 in Mps1-driven generation of the Mitotic Checkpoint Complex (MCC)

To activate the SAC and delay anaphase onset, unattached kinetochores produce the MCC, which is a complex of four proteins: the 'closed' form of Mad2, Cdc20, BubR1 (Mad3 in budding yeast), and Bub3. MCC production is licensed by the Mps1 kinase, which according to current understanding, sequentially phosphorylates the 'MELT' motifs in Spc105/Knl1, Bub1, and then Mad1, to license the interaction between Spc105/Knl1 and Bub1-Bub3, Bub1 and Mad1, and Mad1 and Cdc20 respectively (Figure 1A) [3-6]. Cdc20 is also recruited by Bub1 and BubR1 through their constitutive, Mps1-independent interactions [17]. This recruitment of SAC signaling proteins to the kinetochore is essential for SAC activation.

Although Mps1 plays the dominant and essential role in SAC signaling, Aurora B kinase activity is also required for maximal signaling [9-11, 18-23]. In budding yeast, Aurora B phosphorylates Mad3/BubR1 [24]. Whether Aurora B phosphorylates other SAC signaling proteins to catalyze MCC production is unknown and difficult to determine, mainly because Mps1 and Aurora B act concurrently within unattached kinetochores, and they likely phosphorylate the same proteins. Therefore, to test whether Aurora B phosphorylates one or more SAC proteins to promote MCC generation, we used the ectopic SAC activation assay or "eSAC" [13]. In this assay, Mps1 or just its kinase domain is conditionally dimerized with cytosolic protein fragments containing either the MELT motifs or the Mad1 recruitment domain of Bub1 to drive the SAC signaling cascade in the cytosol [13-16]. By isolating the kinase and its putative substrate in the cytosol, any SAC signaling activity stimulated by of substrate phosphorylation is revealed as delayed mitotic progression. Therefore, this assay is ideal for detecting any direct roles of Aurora B kinase activity in SAC signaling.

Before analyzing putative Aurora B roles in SAC signaling, we used the eSAC assay to clearly delineate the known roles of Mps1 in the SAC signaling cascade (summarized in Figure 1A). For this, we established a simple flow cytometry workflow that monitors cell cycle progression of budding yeast cell cultures. Flow cytometry performed on an asynchronously growing culture of haploid yeast cells reveals two peaks: one corresponding to 1n (G1) and the other corresponding to 2n (G2/M) cells (Figure 1B). When such a culture is treated with a microtubule poison such as nocodazole for ~ 2 hours, the entire cell population shifts to a single peak corresponding to 2n ploidy due to mitotic arrest (Figure S1D). Beyond 2 hours in nocodazole, a

minor 4N peak is also evident. It corresponds to the population of cells that escaped the mitotic block without undergoing cytokinesis. As a positive control, we performed flow cytometry on cells expressing Mps1-2xFkbp12 and a fragment of the Spc105 phosphodomain spanning either one or six MELT motifs that is fused to Frb and GFP (Figure 1B). In both cases, when rapamycin was added to the growth media, the cell population gradually shifted to the 2n peak indicating G2/M arrest (Figure 1B, Figure S1A, rapamycin panels in red) [25]. Inclusion of a Protein Phosphatase I (PP1, antagonizes Mps1) binding site in the phosphodomain did not change the effect of rapamycin (Figure S1A). Most cells became large-budded after two hours in rapamycin and contained two distinct clusters of bioriented sister kinetochores (micrographs in Figure 1B). This morphology is consistent with cell cycle arrest in metaphase [14]. Mitotic arrest upon rapamycin treatment was not observed in cells lacking Mad2 revealing that it was mediated by the SAC (Figure 1B, dashed blue panel). Thus, the gradual shift of the entire cell population to 2n following rapamycin treatment indicates mitotic arrest due to ectopic SAC activation.

Phosphorylated MELT motifs recruit the Bub3-Bub1 complex. Therefore, we next observed cell cycle progression after Mps1 dimerization with either Bub3 or Bub1. In both cases, a prolonged mitotic arrest was observed as expected (Figure S1B). Mps1-Bub1 dimerization did not arrest the cell cycle in cells lacking Mad2 (Figure S1B right), confirming that the observed cell cycle arrest was mediated by ectopic SAC activation [13, 16]. Bub1 contributes two different activities to MCC formation (see schematic at the top of Figure 1C): a central domain (residues 368-609) that binds Mad1 and the conserved ABBA motif ('486-KFNVFENF-496' in yeast) that binds Cdc20 [3, 5, 17, 26, 27]. To separate the contribution of these two activities to MCC generation, we first introduced mutations predicted to abolish Cdc20-binding to the ABBA motif (F490A, V492A, F493A, N495A, referred to as bub1^{-abba}) [26]. Induced dimerization of Mps1 with bub1^{-abba} resulted in ectopic SAC activation suggesting that the ABBA motif is dispensable when ectopic SAC signaling is driven by Mps1 (Figure 1C). Consistent with this observation, *bub1*$^{-abba}$ cells also arrested in mitosis upon nocodazole treatment, although the fraction of cells escaping the mitotic block was higher in these cells compared to wild-type cells indicating that the SAC is weaker (Figure S1D). Mad1-mCherry signal colocalizing with unattached kinetochores in *bub1*$^{-abba}$ cells was also reduced by ~ 50% indicating that mutations in the ABBA motif also affected Mad1 recruitment (Figure S1C) [28]. Bub1-Cdc20 interaction has been difficult to confirm using biochemical methods in HeLa cells [29]. We also could not confirm this interaction in yeast using immunoprecipitation, yeast two-hybrid assays, or microscopy (because fluorescently labeled Cdc20 is not functional, data not shown). However, the conservation of the ABBA motif

sequence and results presented later support our assumption that the *bub1*$^{-abba}$ mutant cannot bind Cdc20.

We next investigated the contribution of Mad1 recruitment via Bub1 to eSAC signaling [3]. Mad1 recruitment is enabled when T453 and T455 in the Bub1 central domain are phosphorylated by Cdk1 and Mps1 respectively [5, 6, 28]. Bub1 contains several additional phosphosites that are also implicated in Mad1 recruitment [3]. Accordingly, mutation of T453 and T455 (bub1$^{T453A, T455A}$) decreased Mad1 recruitment to unattached kinetochores only modestly, and did not affect the strength of SAC signaling in nocodazole-treated cells [30]. Mps1 dimerization with bub1$^{T453A, T455A}$ also resulted in a robust mitotic arrest (Table in Figure S2G). To completely disrupt Bub1-Mad1 interaction, we also mutated Mps1 phosphorylation sites flanking the ABBA motif (e.g., bub1$^{T455A, T485A}$ or bub1$^{T485A, T509A, T518A}$), but these mutations did not affect eSAC signaling driven by Mps1 (Figure S2G). Fluorescence quantification for Mad1-mCherry co-localized with unattached kinetochore clusters following nocodazole-treated in mutant cells showed that Mad1 recruitment was lowered, but not abolished, which explains why eSAC activity persists in these mutants (Figure S1C). Therefore, to completely disable the Bub1-Mad1 interaction, we dimerized Mps1 with bub1-15A, a Bub1 mutant wherein 15 phosphorylation sites (T485, T486, T487, T488, T509, T518, S537, S539, S540, T541, T555, T556, T558, T566 and S578) are non-phosphorylatable [3, 16]. bub1-15A localized to unattached kinetochores in nocodazole-treated cells as well as, or better than, wild-type Bub1. However, it did not activate the SAC (Figure S1D-E, flow cytometry right panel). eSAC activity was also abolished in this mutant (Figure 1C bottom). Taken together, these data show that eSAC signaling mediated by Mps1-Bub1 dimerization requires the Bub1-mediated recruitment of Mad1, but not Cdc20.

Mps1 also phosphorylates Mad1 to allow it to interact with Cdc20 and facilitate the formation of Cdc20:C-Mad2 [5, 6]. Therefore, we next dimerized Mps1 with Mad1 to determine whether this is sufficient to drive ectopic SAC activation. Induced dimerization of the two proteins arrested yeast cells in mitosis, and the arrest was not observed in *mad3Δ* cells indicating that it was mediated by ectopic SAC activation (Figure 1D). eSAC activity persisted in *spc105-6A* cells, wherein all six MELT motifs are non-phosphorylatable and in *bub3Δ* cells. Thus, the ectopic SAC activation does not require Bub1 localization to the kinetochore. The latter observation also indicates that the budding yeast MCC can be formed ectopically without Bub3 [31]. Consistent with the dispensability of the ABBA motif in Bub1 for Mps1-driven SAC signaling, Mps1-Mad1 dimerization produced a robust mitotic arrest in *bub1*$^{-abba}$ cells indicating that Mps1 can phosphorylate Mad1 to promote the Mad1-Cdc20 interaction (Figure 1D). Finally, dimerization of

Mps1 with mad1-4A, wherein residues in Mad1 implicated in its interaction with Cdc20 are non-phosphorylatable [T624A, T704A, T737A, and T739A, displayed in the schematic in Figure 1D], did not arrest the cell cycle [5, 6]. Thus, Mps1-mediated phosphorylation of Mad1 enables Mad1 to interact with Cdc20 and catalyze formation of the Cdc20:C-Mad2 dimer. Interestingly, Mps1-Mad1 dimerization did not affect cell cycle progression in cells expressing *bub1-15A* (Figure S1F). This observation indicates that the scaffolding provided by Bub1 for Mad1 and Cdc20 plays an essential role in the ectopic MCC assembly [32, 33].

The data so far delineate the roles of Mps1, Bub1, and Mad1 in promoting the formation of Cdc20:C-Mad2. MCC formation also requires BubR1, known as Mad3 in in yeast. In metazoa, BubR1 is recruited to the kinetochore by Bub1 [34, 35]. Bub1-BubR1 interaction is also essential for SAC signaling in fission yeast [16]. However, bioinformatic analysis suggests that this interaction is not conserved in budding yeast [36]. Nonetheless, to test whether BubR1 is recruited to unattached kinetochores via an unanticipated mechanism, we fused GFP to the N-terminus of Mad3 (C-terminal fusion of GFP to Mad3 makes it incompetent in SAC signaling, data not shown) and visualized it in nocodazole-treated cells. GFP-Mad3 rarely colocalized with unattached yeast kinetochore clusters, even when significantly over-expressed (Figure 1E, also see Figure S1G). Thus, budding yeast kinetochores mainly catalyze Cdc20:C-Mad2 formation.

These observations suggest the following model for Mps1-driven SAC signaling in budding yeast. As established by previous studies, Mps1 licenses the recruitment of Bub1-Bub3 by phosphorylating the MELT motifs in Spc105/KNL1, and then, the recruitment of Mad1-Mad2 by phosphorylating Bub1. In facilitating MCC production, Bub1-Bub3 mainly serves as a receptor for Mad1-Mad2; the recruitment of Cdc20 via Bub1 may contribute to MCC formation, but it is not essential (Figure 1D, also see S1D for controls). Mps1 also phosphorylates Mad1 to license its interaction with Cdc20, and this is essential for MCC formation. Finally, Mad3 does not localize to yeast kinetochores implying that Cdc20-C-Mad2 binds Mad3 in the nucleoplasm and/or cytosol to form the MCC.

Testing whether Aurora B/Ipl1 kinase activity promotes MCC formation

The Aurora B kinase, known as Ipl1 in budding yeast, is implicated in SAC signaling. In budding yeast, a temperature-sensitive mutant of Ipl1 (*ipl1-1*) rescues the viability of the *spc105*^{RASA} mutant, which otherwise cannot grow because of a severe defect in SAC silencing [37]. By co-localizing with unattached kinetochore clusters in nocodazole-treated budding yeast cells

(Figure 2A, [38]), Ipl1 is positioned to act on SAC proteins that are recruited to the kinetochore by Mps1 activity. Therefore, we hypothesized that Ipl1, like Mps1, phosphorylates Spc105/KNL1, Bub1, or Mad1 to contribute to MCC formation.

To test our hypothesis, we conditionally dimerized Ipl1 with either a fragment of Spc105 spanning its six MELT motifs, full-length Bub1, or full-length Mad1. In each case, we used flow cytometry to monitor cell cycle progression after the addition of rapamycin to growth media. Rapamycin-induced dimerization of Ipl1 with the Spc105 fragment spanning the six MELT motifs had no detectable effect on the cell cycle, but its dimerization with either Bub1 or Mad1 resulted in a cell cycle arrest (Figure 2B). Visualization of fluorescently labeled kinetochores in these cells revealed a morphology consistent with metaphase arrest: large-budded cells with an intact spindle and two distinct, bioriented kinetochore clusters (micrographs in Figure 2B). Importantly, Ipl1-Bub1 dimerization had no discernible effect on cell cycle progression in *mad1Δ* mutants (Figure 2B blue curve in the middle panel). Thus, the observed arrest required a functional SAC.

Ipl1 activity is required to correct monopolar attachments, and therefore, its induced dimerization with SAC proteins, e.g., Bub1, may retard kinetochore biorientation. To ensure that Ipl1 is available for error correction, we created a strain that expresses Ipl1 and Ipl1-Fkbp12 both. eSAC activity persisted in this strain (Figure 2C top). We also monitored kinetochore biorientation in rapamycin-treated cells expressing Ipl1-Fkbp12 and Bub1-Frb by visualizing the centromere of chromosome IV with the help of a centromere-proximal TetO array and TetR-GFP (Figure S2B). Chromosome IV bioriented efficiently in both control and rapamycin-treated cultures, indicating that the induced dimerization of Ipl1 did not detectably affect kinetochore biorientation.

Next, we tested whether the kinase activity of Ipl1 is required for the observed mitotic arrest by dimerizing a kinase-dead allele of Ipl1, Ipl1^{K133R}, with Bub1 [39]. Flow cytometric analysis revealed that cells expressing Ipl1^{K133R}-Frb and Bub1-1xFkbp12 did not arrest in mitosis upon rapamycin treatment (Figure 2C top). Finally, to confirm that the mitotic arrest resulting from Ipl1-Bub1 dimerization is independent of kinetochores, we used bub1$^{368-609}$ as the phosphodomain. This fragment spans just the central domain of Bub1 and lacks the Bub3-binding 'GLEBS' domain and the kinase domain [40]. As expected GFP-bub1$^{368-609}$-2xFkbp12 did not localize to unattached kinetochore clusters in nocodazole-treated cells (Figure 2C bottom). Importantly, Ipl1 dimerization with GFP-bub1$^{368-609}$-2xFkbp12 robustly activated the SAC.

Next, we affinity purified GFP-bub1$^{368-609}$-2xFkbp12 from DMSO-treated cells and cells treated with rapamycin using GFP-Trap beads (Figure S2A). SDS-PAGE analysis revealed a significantly retarded mobility of the protein affinity-purified from rapamycin-treated cells, indicating that its post-translationally modified (Figure S2A). Mass spectrometry analysis of this protein identified phosphorylation of residues T438, S474, S475, T550, T556, and S596 in the phosphodomain of yeast Bub1 (Table S3). Importantly, these phosphorylations were significantly enriched in rapamycin-treated cells. Our analysis identified only one of the 15 sites implicated in Bub1-Mad1 interaction. Nonetheless, this set of observations show that following its rapamycin-induced dimerization, Ipl1 phosphorylates Bub1, and potentially Mad1, to trigger kinetochore-independent SAC activation.

Intact ABBA motif in Bub1 is essential for the Aurora B/Ipl1-mediated ectopic SAC activation

To understand the molecular mechanisms leading to eSAC activation driven by Ipl1, we tested whether the phosphorylation sites within Bub1 implicated in Mad1 recruitment are essential. Interestingly, when Ipl1 was dimerized with bub1$^{T453A,\ T455A}$, cell cycle progression remained unperturbed indicating that eSAC activity was either significantly decreased or abolished (Figure 2D top). Ipl1 dimerization with bub1^{T453A} (i.e., the Cdk1 consensus phospho-site) with Ipl1 resulted in a cell cycle arrest. Thus, the T455 residue in Bub1 is essential for Ipl1 driven eSAC signaling (Figure S2C left). Bub1(485T) was also similarly critical for Ipl1 driven eSAC signaling (Fig. 2D top, Figure S2C). Given that the same mutations did not affect Mps1-driven eSAC signaling, we tested whether these Bub1 residues play a role in kinetochore-based SAC signaling. Flow cytometric analysis of the DNA content in nocodazole-treated cells expressing these bub1 mutants revealed that the SAC was weakened in *bub1*^{T453A,T455A} and abolished in *bub1*^{T455A,T485A} cells (as judged from the fraction of cells that slipped out of the mitotic block to achieve 4N ploidy, Figure S2D). Taken together, these data suggest that Ipl1 can phosphorylate sites in the Mad1-binding domain of Bub1, and that these sites also contribute to kinetochore-based SAC signaling. Given that there is a significant overlap between the residues in Bub1 that can be phosphorylated by Ipl1 in the eSAC assay and the putative Mps1 phosphorylation sites, we wanted to know if Ipl1-mediated phosphorylation of Bub1 can completely bypass the requirement for Mps1. For this, we dimerized Ipl1 and Bub1 in a strain that expresses an analog-sensitive version of the Mps1 kinase [41]. Ipl1 driven eSAC signaling was abolished

when Mps1 kinase was inhibited (Figure S2E). This key observation indicates that Mps1 must prime Bub1 for Ipl1 activity.

We next tested whether recruitment of Cdc20 via the ABBA motif in Bub1 is essential for Ipl1-driven eSAC signaling. Surprisingly, Ipl1 was unable to drive eSAC signaling when dimerized with bub1^{-abba} (Bub1^{FL} as well as bub1$^{368-609}$), as assessed by flow cytometry (Figure 2D bottom flow cytometry panel). This contrasts with Mps1, which does not require a functional ABBA motif for driving SAC signaling (Figure 1C). Thus, unlike Mps1-driven eSAC activation, Ipl1-driven eSAC signaling requires the ABBA motif in Bub1 to be intact. These data also imply that Ipl1, unlike Mps1, cannot phosphorylate Mad1 to promote Mad1 interaction with Cdc20. To test this, we dimerized Ipl1 and Mad1 in cells that lack Bub1 (*bub1Δ*) or in cells that express either bub1^{-abba} or bub1$^{T485A,\ T509A,\ T518A}$. In each case, rapamycin treatment had no discernible effect on the cell cycle (Figure 2E). Thus, Bub1 is required for eSAC activation induced by the dimerization of Ipl1 and Mad1. These results further indicate that Ipl1 primarily phosphorylates Bub1 to facilitate ectopic MCC assembly.

These data advance the following, direct role for Ipl1 in MCC production. Mps1 activates the SAC signaling cascade by phosphorylating the MELT motifs to license the recruitment of Bub1-Bub3. It also licenses the recruitment of Mad1-Mad2 and Cdc20 by phosphorylating Bub1 and Mad1 respectively. Ipl1 kinase also localizes within unattached kinetochores. However, it cannot activate the SAC on its own because it cannot phosphorylate the MELT motifs [13, 14]. After Mps1 phosphorylates the MELT motif and primes Bub1 for Mad1 recruitment, Ipl1 can phosphorylate Bub1 to further promote Mad1-Mad2 recruitment. Importantly, Ipl1 cannot phosphorylate Mad1 to enable the Mad1-Cdc20 interaction; it must cooperate with Bub1 to promote MCC formation [32, 33].

At this juncture, it is important to note two properties of the eSAC system that likely accentuate its effect on the SAC. First, we labeled the genomic copy of Ipl1 with Frb, which means that depending on their relative abundance nearly all Ipl1 or the Fkbp12-tagged SAC signaling protein will be dimerized. Second, the high affinity dimerization of Fkbp12 and Frb domains in the presence of rapamycin will allow Ipl1 to maximally phosphorylate the signaling protein. Consequently, the eSAC system will likely reveal the maximal contribution that Ipl1 can make to SAC signaling. Under physiological conditions, this Ipl1 role is likely to be significantly smaller. Consistent with this, the SAC strength in nocodazole-treated budding yeast cells remains unchanged even when Ipl1 kinase activity is significantly reduced [42].

Evidence supporting a direct role of Aurora B/Ipl1 in driving MCC assembly in kinetochore-based SAC signaling

To detect the contribution of Ipl1 to kinetochore-based SAC signaling, two conditions must prevail. First, Mps1 activity in the kinetochore must be minimal so that effects of Ipl1 activity can be detected. Second, Bub1 must still be recruited to the kinetochore so that the kinetochore localized Ipl1 can act on Bub1 to facilitate MCC formation. As an appropriate model for these conditions, we used cells expressing *spc105*^{RASA}, a well-characterized mutant of Spc105 wherein the highly conserved 'RVSF' motif in the N-terminus is inactivated, which prevents the mutant protein from recruiting Protein Phosphatase 1 (PP1). In yeast cells expressing *spc105*^{RASA}, the SAC remains active in metaphase even after kinetochore biorientation, because PP1 activity in the kinetochore is greatly diminished [30, 37, 43]. As a result, MELT motifs remain phosphorylated even after the formation of stable kinetochore-microtubule attachments, and Bub3-Bub1 remains bound to the MELT motifs [14]. The concurrence of persistent Bub1 recruitment to the kinetochore with diminished Mps1 activity sets up the requisite conditions for observing the hypothesized contribution of Ipl1 to SAC signaling. Indeed, the study by Rosenberg et al. found that a hypomorphic, temperature-sensitive mutant of Ipl1 suppresses the SAC-mediated lethality of *spc105*^{RASA} cells wherein the recruitment of PP1 for SAC silencing is abrogated. This observation implicates Ipl1 kinase activity in the persistent SAC signaling.

Our eSAC experiments show that the ABBA motif in Bub1 is necessary for Ipl1 mediated, but not for Mps1-mediated, SAC signaling. Therefore, we tested whether the ABBA motif in Bub1 is necessary for the persistent SAC signaling in the *spc105*^{RASA} cells. Using tetrad analysis, we found that the *bub1*$^{-abba}$ *spc105*^{RASA} double mutant is viable, indicating that the Bub1 ABBA motif is essential for the persistent SAC signaling from bioriented kinetochores occurring in the *spc105*^{RASA} cells (Figure 2F, left). As expected, *bub1*$^{-abba}$ mutation did not detectably alter SAC strength in nocodazole-treated yeast cells, wherein Mps1 activity within unattached kinetochores is maximal (Figure 2F, right). We also observed similar rescue of *spc105*^{RASA} by *bub1*$^{T455A,\ T485A}$ and *bub1*$^{T485A,\ T509A,\ T518A}$ (Figure S2F and bub1^{T453A,T455A}, also see ref. [30]). These genetic interactions imply that the Bub1-mediated recruitment of both Mad1 and Cdc20 is necessary for the persistent SAC signaling from bioriented kinetochores in cells expressing *spc105*^{RASA}. Note that we very rarely observed background mutations that rescue the lethality of *spc105*^{RASA}. Combined with the suppression of *spc105*^{RASA} lethality by *ipl1-1* (temperature sensitive mutant of Aurora B/Ipl1 in yeast), these data support our hypothesis that Ipl1 directly

promotes MCC formation by phosphorylating Bub1 to promote Mad1 recruitment and relying on the ABBA motif in Bub1 for Cdc20 recruitment.

Ipl1 may phosphoregulate the Cdc20 recruited by Bub1 to promote SAC signaling. Therefore, we tested whether any of the putative phosphorylation sites in Cdc20 are necessary for SAC signaling using the rescue of *spc105*^{RASA} mutant viability as the readout. We created several phospho-null alleles of Cdc20 by mutating residues (S24, S46, S52, S62, S88, S89, S229, S602-S605) that are either known or likely to be phosphorylated (www.phosphosite.org). Tetrad analysis of diploid double mutants carrying *spc105*^{RASA} and the Cdc20 mutants showed that none of the mutations that we tested suppressed the lethality due to *spc105*^{RASA} (data not shown). These results suggest that the phosphorylation of Cdc20 is not essential for SAC signaling.

Aurora B drives ectopic SAC signaling in human cells

In human cells, Aurora B promotes SAC signaling indirectly by: (1) creating unattached kinetochores, (2) potentiating Mps1 recruitment to the kinetochore [10], and (3) inhibiting phosphatase activity antagonizing Mps1 in the kinetochore [9]. A direct involvement of Aurora B kinase activity in SAC signaling has also been noted before. In human and fission yeast cells, Aurora B kinase activity is required for SAC signaling initiated by artificial tethering of Mad1 to bioriented kinetochores [44-46]. Interestingly, Bub1 is also essential for SAC activation under these conditions [47], similar to the requirement of Bub1 when Aurora B and Mad1 are dimerized in yeast cells (Figure 2D). In fission yeast cells containing unattached kinetochores, Aurora B activity is necessary for maintaining mitotic arrest induced by unattached kinetochores, indicating that the creation of unattached kinetochores is not its only role in SAC signaling [21]. Based on these observations and considering our budding yeast data, we hypothesized that Aurora B contribute to SAC signaling by phosphorylating Bub1 in human cells.

For this work, we adapted the previously described eSAC system in HeLa cells [13]. Briefly, we created HeLa cell lines that constitutively express one of three protein fragments: a KNL1 (Spc105 homolog) phosphodomain containing six MELT motifs (two tandem copies of a fragment spanning three motifs in KNL1 also named as M3-M3; [48]), the central domain of Bub1, or the C-terminal domain of Mad1, each fused to mNeonGreen-2xFkbp12 (Figure 3A, Methods). In these cells, we conditionally expressed Frb-mCherry-INCENP$^{818-918}$ using a doxycycline-induced promotor. INCENP$^{818-918}$ (known as INBox) binds to and is essential for the

activation of Aurora B in human cells [49]. As expected, the INCENP fragment was cytosolic, and did not show detectable localization at kinetochores (Figure S3A). Due to the acute induction of the inducible promoter (< 48 hours prior to the start of the experiment, see Methods), the expression level of Frb-mCherry-INCENP$^{818-918}$ was lower than that of the Fkbp12-fused SAC protein fragment, and it varied from cell to cell (see Figure 3A). This variability allowed us to measure both the dose (amount of conditionally dimerized complex determined by the average mCherry fluorescence in a mitotic cell) of the Aurora B-based eSAC and the cellular response to the eSAC dosage in the form of delayed anaphase onset.

To study effects of the induced dimerization of Frb-mCherry-INCENP$^{818-918}$ with each of the three protein fragments, we added rapamycin to the growth media for asynchronously growing HeLa cells and imaged them for a period of ~ 24 hours (Methods). For cells that entered and completed mitosis during this period, we determined the mitotic duration as the time duration for which a HeLa cell exhibits with the rounded morphology characteristic of mitotic cells, before undergoing anaphase onset (Figure 3B). In each mitotic cell, we quantified the average mCherry signal over the entire cell and used this value as the reporter of eSAC dosage [13].

The rapamycin-induced dimerization of Frb-mCherry-INCENP$^{818-918}$ with mNeonGreen-2xFkbp12 (no SAC signaling activity) did not affect the duration of mitosis (Figure 3D), indicating that the over-expression of INCENP$^{818-918}$ the recruitment of endogenous Aurora B away from its normal functions for eSAC activity does not significantly affect mitosis. Dimerization of INCENP$^{818-918}$ with the fragment of KNL1 containing six MELT motifs also did not affect mitotic progression (Figure 3B, left, supporting Video S1). Consistently, western blot analysis of the whole cell lysates probed with a phospho-specific antibody against 'MEIpT' showed that the MEIT motifs (variants of the consensus 'MELT' sequence) in this fragment were not phosphorylated upon its dimerization with INCENP$^{818-918}$ (Figure 3C, also see Figure S3B and S3C). Dimerization of INCENP$^{818-918}$ with either Bub1$^{231-620}$ or Mad1$^{479-725}$ resulted in a dose-dependent mitotic delay (Figure 3B, middle and right, supporting Videos S2-S3). In both cases, we quantified the maximal response as the plateau of the 4-parameter sigmoid fit to the mean values of binned data (Figure 3D, Methods). The maximal mitotic delays induced by the dimerization of Frb-mCherry- INCENP$^{818-918}$ with Bub1$^{231-620}$ and Mad1$^{479-725}$ were similar in magnitude, and also comparable to the maximal delays caused by the dimerization of the Mps1 kinase domain with the same protein fragments (Figure 3D; data marked with an asterisk are reproduced from [13] for comparison). This is indicative of the similar activity of the eSAC

systems. Thus, Aurora B can drive ectopic SAC signaling by phosphorylating either Bub1 or Mad1, or both, in HeLa cells.

We also tested whether the Aurora B driven eSAC activity is kinetochore independent. We fused Fkbp12 to Bub1$^{271-620}$ that cannot localize to kinetochores, because it lacks the 'GLEBS' motif that mediates the Bub1-Bub3 interaction and the TPR domain which can interact with Knl1/Spc105 [40, 50]. We created two cell lines expressing Bub1$^{271-620}$-mNeonGreen-2xFkbp12 and either Frb-mCherry-Mps1 kinase domain or Frb-mCherry-INCENP$^{818-918}$. In both cell lines, addition of rapamycin to the growth media resulted in a dose-dependent prolongation of mitosis (Figure 3E left). In fact, the maximal delay was slightly higher indicating that eSAC activity was stronger presumably because the Bub1 fragment does not sequester Bub3, ensuring the full availability of Bub3-BubR1 for MCC formation [51]. We also confirmed that the eSAC activity requires an active Aurora B kinase, because direct dimerization of the kinase domain of Aurora B (residues 61-344), which is inactive on its own, with the Bub1 phosphodomain did not affect the progression of mitosis (Video S4).

Finally, we tested whether the observed mitotic delays are due to ectopic MCC formation. For this, we synchronized HeLa cells expressing INCENP$^{818-918}$ and Bub1$^{231-620}$ in G2/M and then released them into media either with or without rapamycin. In each case, we harvested mitotic cells, prepared clarified cell lysates, and immunoprecipitated Cdc20. We also performed the same assay on cells wherein Mps1 kinase domain is dimerized with Bub1$^{271-620}$-mNeonGreen-2xFkbp12. In both cases, increased amounts of Mad2 co-immunoprecipitated with Cdc20 from lysates made from rapamycin-treated cells compared to DMSO-treated cells (Figure S3D). Thus, the dimerization of INCENP$^{818-918}$ with the Bub1$^{271-620}$ in mitotic cell enhances the generation of Cdc20:C-Mad2 and therefore, the MCC. The increase in Mad2 was greater in the Mps1-driven eSAC system than in the Aurora B driven system. This is likely because Aurora B works downstream from Mps1, and it cannot phosphorylate Mad1.

The ABBA motif of human Bub1 is necessary for the ectopic SAC activation by Aurora B

Our budding yeast data also indicate that Mps1-driven eSAC activity does not require the ABBA motif in Bub1, but Aurora B-driven eSAC activity does (Figure 1C and 2D). To test whether this dependence is conserved in human cells, we created two cell lines that express either Frb-mCherry-Mps1 kinase domain or Frb-mCherry-INCENP$^{818-918}$ along with Bub1$^{271-522}$, which lacks the ABBA motif. In cells expressing the Mps1 kinase domain, addition of rapamycin resulted in a

clear dose-dependent delay in anaphase onset, revealing that the Mps1 kinase domain does not require the ABBA motif in Bub1 to facilitate ectopic MCC assembly (Figure 3E top right and 3F). However, the dimerization of the same fragment with Frb-mCherry-INCENP$^{818-918}$ produced a noticeably weaker response (Figure 3E bottom and 3F). These results mirror the findings from the budding yeast eSAC experiments: the ABBA motif in Bub1 is dispensable for Mps1-driven eSAC activity, but it is necessary for Aurora B-driven eSAC.

The necessity of the ABBA motif in Bub1 for Aurora B-driven eSAC activity also implies that the mitotic delay observed upon Frb-mCherry-INCENP$^{818-918}$ dimerization with Mad1$^{479-725}$ will require Bub1-Mad1 interaction, which is dependent on Mps1 activity. Rapamycin-induced dimerization of INCENP$^{818-918}$ and Mad1$^{479-725}$ failed to delay cell division when the Mps1-inhibitor Reversine was added to the growth media (Figure S3E). Thus, Mps1 kinase activity is still required for eSAC activity induced by INCENP$^{818-918}$ dimerization with Mad1$^{479-725}$.

Aurora B kinase activity promotes MCC assembly during kinetochore-based SAC signaling

Finally, we wanted to test whether Aurora B directly promotes MCC formation from within unattached kinetochores. To this end, we adopted the following strategy. Our eSAC data indicate that Aurora B can promote MCC formation by phosphorylating Bub1 within unattached kinetochores, but only after Mps1 licenses the recruitment of Bub1-Bub3 by phosphorylating the MELT motifs. Therefore, to detect the contribution of Aurora B to MCC formation, the following three conditions must be met: (1) Mps1 must license the recruitment of Bub3-Bub1 to unattached kinetochores and phosphorylate Bub1, so that Aurora B can act on this Bub1, (2) Mps1 activity should be reduced so that the contribution of Aurora B activity can be detected, and (3) PP1 and PP2A must be inhibited to ensure that the MELT motifs remain phosphorylated and thereby retain Bub1-Bub3 [9].

To meet these three conditions, we used the following approach. First, we released G1/S synchronized HeLa cells expressing histone H2B-RFP cells into the cell cycle, and then treated them with nocodazole to depolymerize microtubules. This treatment created cells with unattached kinetochores and active SAC. In these cells, Mps1 kinase activity was partially suppressed using 250 nM Reversine. As a result, Mps1 activity was significantly reduced, but it was still sufficient to license Bub1-Bub3 recruitment in the unattached kinetochores [48]. To satisfy the third condition: lowering PP2A activity within the kinetochore, we suppressed PP2A

recruitment to the kinetochore by RNAi mediated knockdown of the five B56 isoforms that target PP2A to the kinetochore. We also reduced phosphatase activity further by combining the B56 RNAi and treatment with Calyculin A, which inhibits PP1 strongly and PP2A to a lesser extent [52].

Consistent with prior studies, the partial inhibition of Mps1 significantly reduced the duration of the average duration of the mitotic arrests induced by 330 nM nocodazole to 126 ± 100 minutes (mean ± S.D., Figure 4A, compared to > 1000 minutes in cells treated with nocodazole alone, data not shown). Disruption of PP2A recruitment to the kinetochore increased mitotic duration to 258 ± 160 minutes (mean ± S.D., Supporting Video S5) [9]. When Aurora B activity was inhibited by the addition of the small molecule inhibitor ZM447439 under the same condition, the mitotic arrest was completely abolished, and the cells exited mitosis within 20 minutes (15 ± 6 minutes, Supporting Video S6). The addition of Calyculin A did not increase the duration of mitosis (Figure 4A). These experiments indicate that Aurora B kinase activity contributes to SAC signaling directly and independently from its indirect role in retarding SAC silencing.

In summary, our eSAC data reveal that Aurora B can directly promote MCC formation by phosphorylating Bub1, and thereby promoting its interaction with Mad1 (Figure 4B). Importantly, Aurora B does not activate the SAC on its own, primarily because it cannot phosphorylate the MELT motifs in Spc105/KNL1. However, after Mps1 activates the SAC by phosphorylating the MELT motifs to enable Bub1-Bub3 recruitment to the kinetochore and primes Bub1 by phosphorylating it in concert with Cdk1 [5, 6], Aurora B phosphorylates the central domain of Bub1 to promote the recruitment of Mad1-Mad2. Bub1-Mad1 binding in turn coordinates the interaction between Mad1-Mad2 and the Cdc20 molecule recruited by the ABBA motif in Bub1, which ultimately results in the formation of the closed-Mad2-Cdc20 complex, paving the way for MCC formation [32, 33].

The requirement of Mps1 activity upstream from Aurora B in kinetochore-based SAC signaling and the significant overlap among the phosphorylation targets of the two kinases prevented us from testing this model directly. Nonetheless, the model explains prior observations showing that Aurora B cooperates specifically with Bub1 in promoting SAC signaling [18]. We propose that Cdc20 required for Aurora B-mediated MCC formation must be recruited via the ABBA motif in Bub1, because Aurora B cannot phosphorylate Mad1 to promote Mad1-Cdc20 interaction. In contrast, Mps1 phosphorylates Mad1 to license the Mad1-Cdc20 interaction to enables MCC formation [17, 18, 53]. Therefore, Bub1 and its ABBA motif are both essential for Aurora B's contribution to SAC signaling.

This role of Aurora B in directly promoting SAC signaling is likely be physiologically significant, especially under conditions wherein Mps1 activity in the kinetochore is weakened. One such situation is dividing cells containing kinetochores with end-on, but syntelic, attachments (Figure 4C). End-on attachments are sufficient to suppress Mps1 activity [54-57] and weaken Mad1 recruitment via the core SAC signaling cascade and possibly through the fibrous corona [58]. Despite lowered Mps1 activity in these kinetochores, Aurora B, which is enriched at these kinetochores, can promote MCC formation by phosphorylating Bub1, delay anaphase onset, and thereby reduce chromosome missegregation. Consistent with this model, Aurora B and the ABBA motif in Bub1 are both essential for SAC signaling specifically in Taxol-treated cells, wherein kinetochores maintain end-on attachments [17, 18]. This direct role of Aurora B in SAC signaling may also contribute to the positive correlation observed between centromeric tension and SAC signaling.

Acknowledgements

This work was funded by the 5R35-GM126983 from NIGMS to APJ. We thank Prof. Mara Duncan and her lab (Department of Cell and Developmental Biology, University of Michigan Medical School) for their help. We acknowledge all the Joglekar lab members for their constructive criticism. We specially thank our past lab member Alan A. Goldfarb who did the initial pilot assay to show that rapamycin induced dimerization of Mps1-FRB with Mad1-Fkbp12 arrests the cell cycle. The authors acknowledge that this work would not have been possible without the HeLa cell line, which was developed from Henrietta Lacks' cells taken without compensation or informed consent.

Competing interests

We declare that no competing interests exist.

Figure Legends

Figure 1 Dissection of the regulatory role of the Mps1 kinase in the SAC signaling cascade using the 'eSAC' system. (A) A simplified schematic of the SAC signaling cascade in budding yeast. Black arrows represent regulated recruitment of downstream signaling proteins; black lines represent constitutive protein-protein interactions. The 'Mps1' label over an arrow signifies phosphoregulation of the protein recruitment step by Mps1. Gray arrow represents the assembly of sub-complexes into the mitotic checkpoint complex. (B) The ectopic activation of the SAC signaling cascade (simplified on the left hand) by the rapamycin-induced dimerization of Mps1-2xFkpb12 with a cytosolic fragment of Spc105 containing just one MELT motif (GFP-Spc105$^{120\text{-}128}$-Frb). Graphs on the right show the quantitation of cellular DNA content using flow cytometry over 4 hours after the addition of rapamycin to the growth media. Strain genotype is indicated at the top of each graph. Grey, red and dashed blue lines show cytometry results for DMSO-treated, rapamycin-treated wild-type and *mad1Δ* cells respectively. Representative micrographs of yeast cells expressing the indicated, fluorescently labeled proteins (right). Notice that the cytosolic GFP-Spc105$^{2\text{-}128}$-Frb displays faint kinetochore colocalization in rapamycin-treated cells, likely because Mps1 localizes to bioriented kinetochores [14]. Scale bar~3.2µm. (C) Top: Domain organization of full length Bub1 (Bub1^{FL}) and its middle domain in budding yeast. Bottom left: Schematic of the potential effects of the rapamycin-induced dimerization of Mps1-Frb with Bub1-2xFkbp12. Bottom right: Graphs show flow cytometry of DMSO-treated (black lines) and rapamycin-treated (red lines) cells with the indicated genotype. (D) Top: Flow cytometry panels showing effects of rapamycin-induced dimerization of Mps1-Frb with the Mad1-2xFkbp12 in wild-type, in absence of Mad3, in presence of spc105-6A, in absence of Bub3 and in presence of bub1$^{\text{-abba}}$. Plots with black, red and cyan lines indicate cells treated with DMSO (control), rapamycin and nocodazole respectively. Middle: Domain organization of Mad1-CTD (amino acid 426-749) in budding yeast. Bottom: In left, a partial schematic of SAC cascade is shown. In right the potential effects of the rapamycin-induced dimerization of Mps1-Frb with the Mad1-CTD-2xFkbp12 or Mad1-CTD$^{4A\ (T624A,\ T704A,\ T737A,\ T739A)}$-2xFkbp12 are shown. Color scheme as in B-C. (E) Localization of ectopically expressed GFP-Mad3 in cells arrested in mitosis due to nocodazole treatment. Note that in nocodazole-treated yeast cells typically contain two kinetochore clusters. The larger cluster is proximal to the spindle pole bodies (not visualized), and kinetochores within this cluster are attached to short microtubule stubs. The smaller cluster is distal to the spindle pole bodies (asterisk), and the kinetochores within this cluster are unattached [59]. Also see Figure S1. Scale bars ~ 3.2 µm.

Figure 2 Rapamycin-induced dimerization of Aurora B/Ipl1 with Bub1 and Mad1, but not MELT motifs, leads to ectopic SAC activation. (A) Localization of Ipl1-mCherry and yeast kinetochores (visualized with Spc105$^{222::GFP}$) in yeast cells arrested in mitosis due to nocodazole treatment. Asterisks mark the cluster of unattached kinetochores in each cell. Scale bar ~ 3.2µm. (B) Left: Potential effects of the rapamycin-induced dimerization of Ipl1-Frb with the indicated SAC signaling protein. Middle: flow cytometry analysis of DMSO or Rapamycin-treated cultures of indicated strains. Color scheme as in Fig. 1. Right: Micrographs showing morphology of rapamycin-treated cells expressing Ip1-Frb and either Bub1-2XFkbp12 or Mad1-2XFkbp12. Scale bar~3.2µm. (C) Top left: Flow cytometry analysis following rapamycin induced dimerization of Bub1-1xFkbp12 with Ipl1^{WT} (red) or ipl1^{K133R}-Frb-GFP (dashed blue). Top right: Representative micrographs of yeast cells expressing Dsn1-mCherry after treatment with DMSO or rapamycin. Scale bar~3.2µm. Bottom left: Flow cytometry panel showing effects of rapamycin induced dimerization of Ipl1-Frb with GFP-bub1$^{368-609}$-2xFkbp12 (Color scheme: DMSO, grey; WT, red; -abba, dashed blue). Bottom right: Representative micrographs of yeast cells expressing Ndc80-mCherry and GFP-bub1$^{368-609}$-2xFkbp12 after treatment with DMSO, rapamycin and nocodazole. Scale bar~3.2µm. (D) Dissection of the contributions of Bub1-mediated recruitment of Mad1 and Cdc20 in ectopic SAC signaling driven by Mps1 using Bub1 point mutants. 2xFkbp12-tagged Bub1 mutants (indicated at the top of each flow cytometry panel) expressed from the genomic Bub1 locus. (E) Flow cytometric analysis of the effect of rapamycin induced dimerization of Ipl1 and Mad1 in absence of Bub1 (*bub1Δ*, top), in presence of bub1^{-abba} (middle) and in presence of bub1$^{T485A, T509A, T518A}$ (bottom) on the cell cycle. (F) Left: Tetrad dissection of diploids with the indicated genotype. The plate with *SPC105/Δ, spc105^{RASA}* were imaged after 2 days (left) and 5 days (middle) before replica plating. The plate with *SPC105/Δ, spc105^{RASA}*, *bub1^{-abba}* was replica plated after 2 days of incubation and then imaged on the 3rd day. The growth rate of segregants expressing *spc105Δ*, *spc105^{RASA}, bub1^{-abba}* (red circles) is similar to wildtype segregants. The numbers of inviable segregants for *spc105Δ*, *spc105^{RASA}, bub1^{-abba}* and inviable or micro-colony forming segregants (blue squares) for *spc105Δ*, *spc105^{RASA}* are consistent with the probabilities predicted by the random segregation of three and two genes (0.33 and 0.5) respectively. Right: Flow cytometric analysis of cell cycle progression in nocodazole-treated cells carrying the indicated mutations.

Figure 3 Rapamycin-induced dimerization of INCENP$^{818-918}$ with Bub1 and Mad1, but not with MELT motifs, leads to ectopic SAC activation in HeLa cells. (A) Left: Schematic of the eSAC system designed to test the roles of Aurora B kinase activity in the core SAC signaling cascade in HeLa cells. Right: A representative micrograph from a time-lapse experiment

showing the variable expression of Frb-mCherry-INCENP$^{818-918}$. Scale bar ~ 8.25 microns. (B) Schematic at the top displays the domain organization of the eSAC phosphodomain. Scatter plots show the correlation between time in mitosis for a given cell and the average mCherry fluorescence at the beginning of mitosis for that cell. Each gray dot represents one cell (n = 520, 787, 840 respectively, data pooled from 2 experiments). The blue circles represent the mean of data binned according to the mCherry signal; the horizontal and vertical lines represent the s.e.m. For the Bub1 and Mad1-CTD fragments, the solid blue lines display a four-parameter sigmoidal fit to the binned mean values; R^2 values = 0.2, 0.2, respectively. (C) Western blot probing for the phosphorylation of the MEIT motif by Aurora B. Also see Figure S3C. (D) Bar graphs display the maximal response predicted by the 4-parameter sigmoidal fit from B. Vertical lines display the 95% confidence interval for the estimated maximal response. For comparison, the maximal response from eSAC systems comprised of the same three eSAC phosphodomains dimerized with the Mps1 kinase domain is also plotted (data marked by asterisks reproduced from [13]). Vertical lines for the M3-M3-Mps1 dimerization represent the standard deviation of the bin corresponding to the peak eSAC response. This representation was made necessary by the non-monotonic nature of the dose-response data. (E) The contributions of the Bub3- and Cdc20-binding domains in Bub1 to the observed eSAC activity driven by either the Mps1 or Aurora B (n = 2635, 614, for the top panel and n = 752, 1524 for the bottom panel; R^2 values = 0.44, 0.24, 0.51, and 0.16 respectively pooled from at least 2 experiments). The domain organization of the phosphodomain is displayed in the schematic at the top. Data presented as in B. (F) Comparison of the maximal response elicited from the indicated phosphodomains by either the Mps1 kinase domain or INCENP$^{818-918}$ (predicted mean ± 95% confidence intervals).

Figure 4 Aurora B contribution to kinetochore-based SAC signaling. (A) Scatter plot displays the duration of the mitotic arrest. Experimental treatments are indicted below each bar. (n = 92, 48, 43, 44, 41, experiment performed twice). Cells treated with B56 RNAi and ZM447439 both exited from mitosis very rapidly without assuming the rounded morphology. In this case, entry of the cell into mitosis was visually identified by the release of surface adhesion along with concurrent condensation of Histone H2B signal (in one experiment). Exit from mitosis was identified from the re-spreading off the cell over the surface (micrograph montage at the bottom, also see Supplementary Video S5). Scale bar ~ 9 microns. (B) Table summarizes the results from the eSAC experiments performed both in yeast and human cells. (C) The proposed mechanism of the direct role of Aurora B kinase activity in SAC signaling. (D) Aurora B-

mediated promotion of MCC generation may enable kinetochores with syntelic attachments to continue to produce MCC and thus delay anaphase onset.

Supplementary Figure legends

Figure S1 - Analysis of the Mps1 kinase mediated SAC signaling cascade using the 'eSAC' system. (A) Flow cytometry-based analysis of cell cycle progression following rapamycin-induced dimerization of Mps1-Fkbp12 with either GFP-Spc105$^{120-329}$-Frb (red), which contains six MELT repeats, or GFP-Spc105$^{2-329}$-Frb (dashed blue), which contains the Glc7 recruitment domain along with the six MELT repeats. **(B)** Left: Flow cytometric analysis of cell cycle progression following the rapamycin-induced dimerization of Bub3 and Mps1 in wild-type cells. Right: Flow cytometry analysis following the rapamycin-induced dimerization of Bub1 and Mps1 in wild-type (red) and *mad2Δ* cells (dashed blue). (**C**) Left: Representative images of cells with unattached kinetochore clusters showing co-localization of the indicated proteins with fluorescently labeled kinetochores (Spc105$^{222::GFP}$ and Ndc80-GFP for WT and bub1^{-abba} respectively). Note that the Mad1-mCherry puncta marked with an asterisk result from the deletion of the nuclear pore protein Nup60. These puncta are not associated with kinetochores. Mad1 puncta co-localizing with kinetochores are marked with arrowheads. Scale bar ~3.2µm. Right: Scatter plot shows the quantification of fluorescence signal of kinetochore-localized Mad1-mCherry (mean±s.e.m., normalized to the average signal measured in nocodazole-treated wild-type cells). n=146, 151, 21 and 73 for WT, bub1^{-abba}, bub1$^{T455A, T485A}$ and bub1$^{T485A, T509A, T518A}$ respectively pooled from two different technical repeats. The p values obtained from pairwise t-test analyses performed on the data are mentioned in the top of the plot. **(D)** Left: Effect of nocodazole treatment on cell cycle progression in *bub1Δ* (left), bub1^{-abba} (2nd from the left) and bub1-15A (2nd from the right) cells. Right: Scatter plot showing quantification of fraction of 4N population in WT, bub1^{-abba} and *bub1Δ* cells. The p values derived by pairwise t-tests performed on the data are mentioned on the top of the graph. **(E)** Left: Representative microscopic images showing localization of bub1-15A-mCherry and unattached kinetochores (visualized by Ndc80-GFP) in yeast cells arrested in mitosis due to nocodazole treatment. Scale bar ~3.2µm. Right: Scatter plot shows the quantification of fluorescence signal of bub1-15A-mCherry (mean+s.e.m., normalized to the average signal measured in nocodazole-treated wild-type cells). n=115 and 108 for WT and bub1-15A respectively pooled from two different technical repeats. We performed Mann Whitney test on the data. The p-value is depicted above the plot. (**F**) Effect of nocodazole, rapamycin and DMSO (control) treatment on cell cycle

progression in strain expressing Mps1-Frb, Mad1-2xFkbp12 and bub1-15A-mCherry. **(G)** Left: Western analysis by α-GFP and α-Tubulin (loading control) on the lysate of Mad1-GFP, GFP-Mad3 and cells wherein GFP-Mad3 is overexpressed. Right: Flow cytometry to test the effect of nocodazole treatment on either GFP-Mad3 (left), GFP-Mad3 overexpression (middle) or *mad3Δ* cells (right).

Figure S2- Dissection of the contribution of Aurora B/Ipl1 in SAC activation. (A) GFPTrap purification of GFP-bub1$^{368-609}$-2xFkbp12. Image of a Coomassie stained gel following the affinity purification. Expected molecular weight of GFP- bub1$^{368-609}$-2xFkbp12 is approximately 79.0 kDa. The blue rectangles indicate the region incised and processed for mass spectrometry. **(B)** Left: Bar graph summarizes the scoring of cells based on chromosome 4 segregation (observed by TetR-GFP bound to TetO array adjacent to centromere 4/*CENIV*) and spindle morphology (Spc98-mCherry). The scoring key is displayed on the right. The number of cells scored for the analysis: n = 110 and 282 for control and rapamycin-treated cell samples respectively, pooled from three technical repeats performed on two biological replicates). Scale bar in the inset images: ~3.2 µm. Arrowheads depict the location of *CENIV-TetO* foci. **(C)** Effect of rapamycin induced dimerization of Ipl1 with either bub1^{T453A} (left) or bub1$^{T509A,\ T518A}$ (middle) or bub1T485A, T509A, T518A (right). **(D)** Left: Flow cytometry profile showing cell cycle progression in nocodazole treated cells of indicated strains. Cells expressing bub1$^{T455A,\ T485A}$ transition to 4n ploidy after 4 hours of exposure to nocodazole, suggesting that the mutation weakens, but does not abolish, the SAC (compare with results of a similar analysis on *bub1Δ* cells in Figure S1D). Right: Scatter plot depicting the fraction of cells with 4N ploidy after 4 hours of nocodazole treatment (genotypes indicated below the X axis). The data were accumulated from at least three independent flow cytometry experiments. The statistical significances were derived by pairwise t-tests and p values are mentioned at the top. (**E**) Top: Flow chart describes the workflow to inactivate Mps1 prior to dimerize Ipl1-Frb-GFP with Bub1-1xFkbp12. Bottom left: Bar graph depicts the fraction of mitotic when the cells expressing analogue sensitive Mps1 were treated with rapamycin and 1-NMPP1 as mentioned in the graph. Bottom right: representative images of prometaphase, metaphase and anaphase cells as observed in untreated (DMSO) and rapamycin treated cells. The number of cells analyzed in each of these 4 treatments: n=366, 461, 246 and 974 respectively. The whole experiment was replicated four times. The statistical significances were derived by 2-way ANOVA test and p values for fractions of anaphase cells are mentioned at the top of the graph. Scale bar ~3.2µm. (**F)** Tetrad dissection analysis of the indicated strains. Please see method section for detailed description

of sporulation, isolation of tetrads and obtaining segregants. (**G**) Table summarizes our observations obtained from the eSAC experiments performed in yeast.

Figure S3- Rapamycin-induced dimerization of INCENP$^{818-918}$ with bub1$^{231-620}$ requires Mps1 function to mediate SAC activation. (A) Representative confocal image shows localization of Hec1 (visualized by anti-Hec1^{9G3} staining) and Frb-mCherry-INCENP$^{818-918}$. Cells were treated with 15 nM GSK923295, a small-molecular inhibitor of the mitotic kinesin CENP-E, for 3 h before fixation to enrich the mitotic population. Scale bar~1.462 µm. **(B)** Control western blot analysis for the phosphorylation of the MEIT motif by Mps1**.** The assay was repeated twice. Molecular weight markers are mentioned on the right. **(C)** Immunoblot assay to analyze phosphorylation of MEIT motif by Aurora B (Frb-mCherry-INCENP$^{818-918}$). Three biological replicates were run in this gel. Here we treated the cells as indicated in the figure. As a control, we ran the lysate of doxycycline and rapamycin treated cells that express Frb-mCherry-Mps1 kinase and M3-M3-mNeongreen-2xFkbp12. Top blot was probed with α-MEITp antibodies and bottom one was probed with α-βTubulin antibodies. The molecular weight markers are mentioned on the right. **(D)** Co-immunoprecipitation of Mad2, BubR1 and Apc3 with Cdc20 in Hela cell lines where we induced rapamycin mediated dimerization of Mps1 and Bub1 or Aurora B and Bub1. Numbers below Cdc20 and Mad2 lanes indicate the mean band intensities relative to that of DMSO treated samples (-rap control). Mad2 intensities were also normalized by Cdc20 band intensities. The experiment was replicated thrice. Mad2 (molecular weight 23.5 kDa, according to Uniprot) runs close to IgG light chain (marked with asterisk. In samples involving Frb-mCherry-Mps1, we observed an extra band for BubR1 that we did not see in samples with Frb-mCherry-INCENP$^{818-918}$. **(E)** Partial inhibition of Mps1 due to Reversine treatment (250 nM, blue line) abolishes eSAC activity induced by the dimerization of INCENP$^{818-918}$ with Mad1$^{479-725}$(n = 154, experiment performed once). Red points and line show DMSO treated cells (data re-plotted from Figure 3B).

Supplementary Videos Legend

Video S1 – Effect of rapamycin induced dimerization of Frb-mCherry-INCENP$^{818-918}$ and M3-M3-mNeonGreen-2xFkbp12 on the duration of mitosis in HeLa A12 cells (hh:mm). Images acquired on the ImageExpress Nano microscope.

Video S2 – Effect of rapamycin induced dimerization of Frb-mCherry-INCENP$^{818-918}$ and M3-Bub1$^{231-620}$-mNeonGreen-2xFkbp12 on the duration of mitosis in HeLa A12 cells (hh:mm). Images acquired on the Incucyte microscope.

Video S3 – Effect of rapamycin induced dimerization of Frb-mCherry-INCENP$^{818-918}$ and M3-Mad1$^{479-725}$-mNeonGreen-2xFkbp12 on the duration of mitosis in HeLa A12 cells (hh:mm). Images acquired on the Incucyte microscope.

Video S4 – Effect of rapamycin induced dimerization of Frb-mCherry- aurora B$^{61-344}$ and Bub1$^{231-620}$-mNeonGreen-2xFkbp12 on the on the duration of mitosis in HeLa A12 cells (hh:mm). Images acquired on the Incucyte microscope.

Video S5 – Cell cycle progression of H2B-RFP expressing HeLa A12 cells treated with 330 nM nocodazole, 250 nM Reversine, and a cocktail of siRNA against five B56 isoforms (hh:mm). Images acquired on the Incucyte microscope.

Video S6 – Cell cycle progression of H2B-RFP expressing HeLa A12 cells treated as in S4 and 10 μM ZM447439 (hh:mm). Images acquired on the Incucyte microscope.

Materials and methods

Plasmid and strain construction

The plasmids and *S. cerevisiae* strains and cell lines used in this study are tabulated in supplementary table S1, S2 and S3 respectively. *S. cerevisiae* strains containing multiple genetic modifications were constructed using standard yeast genetics. Proteins tagged with GFP(S65T) and mCherry or yeast codon optimized mCherry were used to visualize kinetochores, spindle pole bodies and SAC signaling components. A 7-amino-acid peptide (sequence: 'RIPGLIN') was used as the linker between the proteins and their C-terminal tags (GFP, mCherry, Frb or 2xFkbp12). The cassettes for gene deletion, gene replacement and C-terminal tags were introduced at the endogenous locus through homologous recombination of PCR amplicons or using linearized plasmids [60]. In the past, we observed a significant strain to strain variation in the intensity of mCherry-tagged kinetochore proteins or checkpoint proteins due to inherent variability of the mCherry brightness. Therefore, we created all Mad1-mCherry strains by crossing the same transformant of Mad1-mCherry (AJY1836 or AJY3741) with other strains. The deletion mutant of *NUP60* always accompanies Mad1-mCherry to disrupt Mad1localization to the nuclear envelopes [61]. This facilitated clearer imaging and quantification of Mad1 localized to the unattached kinetochores without affecting SAC strength.

To create any diploid yeast strains, we mixed overnight grown cultures of two strains of a and α mating types and spotted the cell suspension on a YPD plate, and then incubated the cells for approximately 3-4 hours at 32°C. To induce meiosis or sporulation of the diploid yeast, we transferred stationary phase diploid cells to starvation media (yeast extract 0.1%, Potassium acetate 1%), and we incubated them at RT for 4-5 days.

All the Spc105 mutants that were used in the study, are chimeras of Spc105 and GFP as described previously [30, 43]. Genes encoding the chimeric proteins were introduced using a cassette that consists of the 397 bp upstream and 250 bp downstream sequences of the SPC105 open reading frame as promoter (*prSPC105*) and terminator (*trSPC105*) sequences respectively. We introduced genes encoding GFP (S65T) at the 222nd or 455th amino acid positions of Spc105 by sub-cloning where we introduced an extra *Bam*HI site (Gly-Ser) at the upstream and *Nhe*I site (Ala-Ser) at the downstream of the GFP fragment. The plasmids based on pRS305 or pRS306 backbone were linearized by *Bst*EII or *Stu*I before transformations to ensure their integration at the *LEU2* or the *URA3* locus respectively.

To build *bub1* phosphomutants containing plasmids, we used the pSK954 plasmid backbone [62]. pSK954 harbors the *ADH1* transcription terminator cloned within *Asc*I-*Bgl*II sites. We cloned the 500bp upstream sequence that harbors *BUB1* promoter, 3.063kb *BUB1* ORF sequence harboring the designated mutations and 651bp *2xFKBP12* or 705bp yeast mCherry within *Sac*II-*Asc*I site of this plasmid. The ORF and *2xFKBP12* or mCherry are linked by 21bp linker which codes for RIPGILK. We also cloned 350bp downstream sequence of *BUB1* which consists of *BUB1* terminator within *Pme*I-*Apa*I. To build the strains with *bub1* phosphomutant allele, we first created a diploid strain where one copy of *BUB1* was deleted with *NAT1* (AJY6055). The plasmids were digested by *Apa*I and *Sac*I to release 6.279kb fragment which recombined at the deleted bub1 locus replacing the *NAT1* cassette. There are two chimeras that express bub1$^{T453A,\ T455A}$ (pAJ852 and pAJ896). *BUB1* ORF of pAJ852 harbors mutations of 449SR450::TG. However, upon testing there were no discernable phenotypic differences between the strains constructed by pAJ852 and pAJ896. Contrary to Mad1-mCherry strains, we had to build the strains with bub1-15A-mCherry by selecting transformants of *Apa*I-*Sac*I digested pAJ923. Therefore, the difference in intensities between wild-type and bub1-15A observed in figure S1E may not be caused by difference in localization but the result of variation in mCherry intensities among the transformants.

From Biggins lab, we acquired pSB148 which contains *IPL1* ORF flanked 1.0 Kb promoter (*prIPL1*) and 654 bp terminator (*trIPL1*). First we cloned FRB-GFP along with ADH1 terminator within *Age*I-*Sac*I sites to generate a chimera which can express Ipl1-Frb-GFP (pAJ941). Then we cloned a 600 bp fragment which was synthesized by Integrated DNA technologies and harbors kinase dead mutation of Ipl1 (K133R) within *Swa*I-*Age*I sites to build pAJ940. We individually transformed AJY6156 (*fpr1Δ*, *BUB1*-1x*FKBP12-HIS3*, *DSN1*-mCherry-*HYG*) with *Stu*I digests of these plasmids where they can be integrated in *URA3* loci.

Similarly, to construct the mutants of putative phosphorylation sites of Cdc20, we cloned the 506bp upstream sequence containing *CDC20* promoter, 1.833kb *CDC20* ORF sequence harboring the designated mutations within *Sac*II-*Asc*I sites of pSK954. We inserted *Spe*I site (ACTAGT) between the promoter and the ORF sequence. We also cloned 300bp downstream sequence of *CDC20* harboring of *CDC20* terminator within *Pme*I-*KpnI* sites. To build the strains with *cdc20* phosphomutant allele, we first created a diploid strain where one copy of *CDC20* was deleted with *TRP1* (AJY5249). The plasmids were digested by *Kpn*I and *Sac*II to release 4.328kb fragment which recombined at the deleted *cdc20* locus replacing the *TRP1* cassette.

Yeast Cell culture

Yeast strains were grown in YPD (yeast extract 1%, peptone 2%, dextrose 2%) or synthetic media supplemented with 2% dextrose (as per requirement of the yeast strain) at 32°C. At the time of imaging strains with TetR-GFP and *CENIV-TetO*, we supplemented the growth media with uracil (final 40µg/ml) to distinctively observe TetR-GFP bound to *CENIV-TetO* array.

To induce meiosis or sporulation, we grew the diploid yeast strains in YPD overnight to stationary phase. Next day, we pelleted the cells down and resuspended them with starvation media (0.1% yeast extract, 1% potassium acetate, 0.025% dextrose) and incubated 4-5 days at RT. To obtain the strain of interest, we incubated the plates with dissected tetrads for 2-3 days. Segregants with wild-type genotype or those harboring *spc105Δ*, *spc105*^{RASA}, *bub1*$^{-abba/phosphomutants}$ grew within that time period. Infrequently, segregants with *spc105Δ, spc105*^{RASA} form micro colonies after 5-6 days of incubation at 30C (Figure 2F, left). To ensure that background mutations are not responsible for the rescue of *spc105*^{RASA} in *bub1*$^{-abba}$ background, we also back-crossed those segregants with wild-type parent strains (YEF473).

For the experiment involving analog sensitive Mps1, we grew yeast cultures for 3h till they attend mid-log phase. These cultures were treated with Hydroxyurea (100mM final) for 2h 30min to synchronize the cells late S phase. Following that, the cells were washed with YPD and released into either YPD (control) or YPD supplemented with 1-NMPP1 (50µM final). After 15min of incubation with 1-NMPP1, either DMSO (control) or rapamycin (1 µg/ml; to mediate the dimerization of Aurora B/Ipl1-Frb-GFP and Bub1-2xFkbp12) was added to the media. We categorized the mitotic cells as the prometaphase, metaphase and anaphase cells according to the distribution of fluorescently labeled kinetochores within each cell (representative images in Fig. S2E). The unbudded cells were considered as the cells in G1 and thus they were not taken into consideration in our analysis.

Flow cytometry

To perform these experiments, we started from overnight inoculum the designated strains to obtain mid log phase cultures. We supplemented the media with Nocodazole (final concentration 15µg/ml) to depolymerize the spindle microtubules and activate the SAC and rapamycin (1 µg/ml) to induce the dimerization of FRB and Fkbp12 fused proteins [63]. We collected samples containing approximately 0.1 OD_{600} cells at 0, 1, 2, 3 and 4h after addition of

the drug, fixed the cells using 75% ethanol, and stored them in 4°C overnight. Next day, we washed out the ethanol, and treated the cells with bovine pancreatic RNase (Millipore Sigma, final concentration 170ng/µl) at 37°C for 24h in RNase buffer (10mM Tris pH8.0, 15mM NaCl). Then we removed the RNase and resuspended the samples in 1X phosphate buffered saline (pH 7.4) and stored them in 4°C. We incubated these samples in Propidium Iodide (Millipore Sigma, final concentration 5µg/ml in PBS) for at least 1h at RT on the day of the assay. The stained cells were analyzed using the LSR Fortessa (BD Biosciences) in Biomedical research core facility, University of Michigan medical school. We repeated flow cytometry for each strain at least twice. Representative results from one of these experiments are displayed in each panel. The data was analyzed using the FlowJO software and the graphs were adjusted by Adobe illustrator. As a control for SAC null strains, we utilized *bub1Δ* or *mad2Δ* strains which revealed high number of 4N population after 4h of incubation with the nocodazole in media. To display the flow cytometry panels, we used the following color scheme: DMSO treatment, grey; rapamycin treatment, red; rapamycin treatment in different genetic background, dashed blue; nocodazole treatment, sky blue.

Microscopy and image analysis

We used A Nikon Ti-E inverted microscope with a 1.4 NA, 100X, oil-immersion objective for all imaging experiments. We also used the 1.5X opto-var lens to measure Mad1-mCherry intensities. The cells were imaged at room temperature in synthetic dextrose (or synthetic galactose media whenever it was required for the assay) supplemented with essential amino acids to obtain at least 20 microscopic fields at a given time points for any strains. We supplemented the mounting media with nocodazole to image the nocodazole arrested cells. For each field of view, a ten-plane Z-stack was acquired (200nm separation between adjacent planes), and at least 20 fields were acquired in each experiment.

Total fluorescence intensities of kinetochore clusters (16 kinetochores in metaphase) was measured by integrating the intensities over a 6x6 region centered on the maximum intensity pixel. We utilized the median intensity of pixels immediately surrounding or a nearby 6x6 area to correct for background fluorescence. Fluorescence intensity was calculated as described previously [64, 65].

Tissue culture and generation of stable cell lines

Henrietta Lacks (HeLa) cells were grown in DMEM media with 10% FBS, 1% Pen/Strep, and 25 mM HEPES at 37 °C and 5% CO2. Stable cell lines expressing the two eSAC components were generated by integrating a bi-cistronic eSAC plasmid at an engineered loxp site in the HeLa genome according to the protocol described in [66]. Clones with stable integration of the eSAC plasmid were selected using Puromycin (1 ug/ml), and several clones were pooled together to create the cell cultures used in the experiments.

The plasmids used for the stable cell lines were based on the plasmids that have been described previously [13]. Briefly, the phosphodomain was integrated into the constitutively expressed ORF of the plasmid using either *Not*I or *Asc*I and *Xho*I restriction sites. The INCENP$^{818-918}$ fragment was integrated into the conditionally expressed ORF using *Fse*I and *Bgl*II restriction sites.

To conduct dose-response analysis, each eSAC cell line was plated ~ 40-48 hours prior to the start of the experiment in DMEM media without Puromycin. Doxycycline was added at the time of plating to induce the expression of either Frb-mCherry-Mps1 or Frb-mCherry-INCENP$^{818-918}$. Prior to imaging, the cells were washed with PBS. Fluorobrite media with 10% FBS, 1% Pen/Strep with or without Rapamycin were added to each well.

Drug treatments and RNAi for experiments with human cells

To induce the expression of either mCherry-Frb-Mps1 kinase domain or -Incenp$^{818-918}$, doxycycline was added to a final concentration of 2 ug/ml (stock concentration 2 mg/ml in DMSO). To induce the dimerization of protein fragments, Rapamycin was added ~ 1 hour prior to the start of the experiment to a final concentration of 500 nM (stock concentration 500 µM in DMSO). GSK-923295 was added to the final concentration of 15 nM (stock concentration 236 µM). Partial Mps1 inhibition was achieved by adding Reversine to the final concentration of 250 nM (stock concentration 500 µM in DMSO). Nocodazole was added to the final concentration of 330 nM (stock concentration 330 µM in DMSO). ZM447439 was added to the final concentration of 10 µM (stock concentration 3mM in DMSO). Calyculin A was added to the final concentration of 100nM (stock concentration 50µM in DMSO). The cocktail of siRNA against five different B56 isoforms was added to a final concentration of 40 nM (stock concentration 10 µM). The siRNA sequences were obtained from ref. [9].

Long term live Cell Imaging of HeLa cells and Image analysis

Imaging was conducted over a period of 24 hours as described in detail previously [13]. We used either the Incucyte Zoom Live Cell Imaging system (Sartorus Inc.) or the ImageExpress Nano live cell imaging system (Molecular Devices) using 20x Phase objectives. To image cells on the Incucyte system, cells were plated in 12-well plastic tissue culture plates, whereas they were plated in 24-well plate glass-bottom dishes for imaging using the ImageExpress Nano system. Typically, 4 positions were selected within each well for imaging. At each position, one phase, GFP, and mCherry image was acquired every 10 minutes. The exposure time for mCherry image was adjusted to minimize photobleaching while ensuring accurate determination of cellular intensity values. It should be noted that the excitation intensity of the Incucyte instrument declined significantly over the course of this study. Furthermore, a small minority of the experiments were carried out on the ImageExpress Nano microscope, which has excitation sources, optics, and detector that are entirely different from the components of the Incucyte microscope. Therefore, the mCherry intensity values across different experiments are not directly comparable. The duration of mitosis and GFP and mCherry fluorescence per cell were determined using a custom image analysis script implemented by a Matlab graphical user interface as described previously [13].

Immunofluorescence assay

Immunofluorescence assay was performed as described previously (Deluca et al., 2011, J Cell Sci). We plated cells expressing Frb-mCherry-INCENP$^{818-918}$ on a 12mm coverslip until they reached 80% confluence. The cells were treated with 15 nM GSK-923295 for 3 h to activate SAC. During fixation, the cells were pre-extracted with 0.5% Triton X-100 in 0.1 M PHEM (240 mM Pipes, 100 mM HEPES, 8 mM MgCl2 and 40 mM EGTA) and fixed with 4% PFA for 10 minutes. The coverslips were washed three times with 0.1 M PHEM and blocked for 30 min at room-temperature with StartingBolck (Thermo scientific, 37578). Next, the cover slips were incubated in primary antibody [Mouse anti-Hec1 (9G3.23, Novus Biological, NB100-338), 1:3000] over night at 4□ C. Next day, we washed them 4 times with 1xPHEM containing 0.05% Tween-20 and incubated with secondary antibodies [Goat anti-Mouse 488 (Life technologies, A11001), 1: 10000) for an additional 45 min at room temperature in dark. Following that, the coverslips washed again four times and mounted in antifade (ProLong; Molecular Probes).

Immunofluorescence images were taken on a Nikon inverted microscope equipped with a Crest X-Light V2 LFOV25 Spinning Disk Confocal head, and Photometric 95B Prime cMOS camera. For each field of view, 31 Z sections were acquired at 0.2 mm steps using a 100x 3, 1.4 Numerical Aperture (NA) Nikon objective.

Immunoprecipitation of Cdc20

This assay was performed as described in [67]. We plated the cell lines expressing Bub1$^{271-620}$-neon2xFkbp12, Frb-mCherry-Mps1 or Bub1$^{225-620}$-mNeon-2xFkbp12, Frb-mCherry-Incenp$^{818-918}$ till they are at ~ 50% confluence. These cells were synchronized in S phase using double thymidine treatment (final concentration 2.5 mM). At the same time, we supplemented the media with doxycycline (final concentration 2 ug/ml) to induce expression of Frb-mCherry-Mps1 kinase domain or Frb-mCherry-INCENP$^{818-918}$. G1/S synchronized cells were washed with PBS and released into media supplemented with the Cdk1 inhibitor RO-3306 (final concentration 15 nM). After 20 hours, G2-synchronized cells were washed with PBS and released into media supplemented with rapamycin (1 µg/ml) for 4 h.

Mitotic cells were harvested using plate shake-off followed by centrifugation at room temperature/ 1100 rpm/ 5 min. Cells were treated with a volume of lysis buffer (75 mM HEPES, pH 7.5; 150 mM KCl, 1.5 mM $MgCl_2$, 1.5 mM EGTA, 10% glycerol, 1% CHAPS, supplemented with protease inhibitor and phosphatase inhibitor cocktails) added in proportion to the weight of the cell pellet. After a 10 min incubation on ice, total cell lysates were clarified by centrifugation (4□C/ 13,000 rpm for 10 min). The cell lysates were incubated with α-Cdc20 anitbody-conjugated protein G-Sepharose 4B beads (4 µg antibodies per 10 µl of beads, Thermo Scientific, catalog #20399) at room temperature for at least 1 h. After that, the beads were washed three times with lysis buffer and boiled in Laemmli sample buffer.

Affinity purification of bub1 middle domain and mass spectrometry

For this set of experiments, we first grew up the strain expressing Ipl1-Frb and GFP-bub1$^{368-609}$-2xFkbp12 till mid-log phase before supplementing the media with DMSO (control) or Rapamycin, where we incubated the cells for approximately 3 h to mediate dimerization of Ipl1 and GFP-bub1$^{368-609}$. We performed cell lysis followed by incubation with GFP-TRAP beads and subsequent purification of GFP- bub1$^{368-609}$ as described previously [43, 68]. We ran the elutes

in 10% gel for subsequent western blotting with anti-GFP antibody or Coomassie staining (See Figure S2A). We made ~0.5cm incisions in the Coomassie stained gel to cut the bands to give them to University of Michigan proteomics resource facility for tandem mass spectrometry. Mass spectrometry data was filtered to retain peptides/peptide spectrum matches (PSM) with false discovery rate (FDR) <1%. We included the sites and flanking sequences in the table S3. We obtained the peptide abundance for each sample from mass spectrometry. Using the normalized abundances, we calculated the fold change from DMSO to rapamycin which shows the relative enrichment of the phosphopeptides.

Immunoblotting

Western blotting was performed using commercial antibodies. The specifications of antibodies and their dilutions are as follows: Mouse α-GFP, JL-8 [Living Colors], 1: 3,000; mouse α-Ds-Red [SantaCruz Biotechnologies], 1: 2,000; mouse α-βTubulin [Sigma Aldrich, T7816], 1: 15,000; rabbit α-Fkbp12 [Abcam, ab2918], 1: 5,000; rabbit α-PhosphoMELT (MEIpT, MELT13/17) [GenScript], 1: 2000; mouse α-Cdc20 [Santa Cruz Biotechnologies, Sc-13162], 1:500; mouse α-Mad2, 1:1000; mouse α-BubR1, 1:1000; mouse α-Apc3 [BD Biosciences, 610455], 1:1000. The primary antibodies were detected using HRP conjugated secondary antibodies (1: 10,000) per the manufacturer's instructions. The subsequent chemiluminescence was detected using the C600 imager from Azure Biosystems. The band intensities were measured by imageJ.

Statistical analysis

The technical replicates represent the number of times each experiment was performed. The biological replicates are defined as multiple transformants or segregants of the same strain which contain identical genotype. For imaging experiments, the number of cells analyzed for each strain and number of experimental replications is noted in the figure legends. All statistical analysis was performed using GraphPad Prism (version 8). We normalized the data with the mean intensities obtained for wild-type controls in each experiment to prepare the scatter plots of Mad1 intensities. To compare sample means in all other cases, we applied either the t-test or two-way ANOVA test to ascertain the statistical significance of the rest of the data using GraphPad Prism (version 8). The p-values obtained from these tests are indicated in the figures.

References

1. Musacchio, A. (2015). The Molecular Biology of Spindle Assembly Checkpoint Signaling Dynamics. Curr Biol *25*, R1002-1018.
2. Lampson, M.A., and Cheeseman, I.M. (2011). Sensing centromere tension: Aurora B and the regulation of kinetochore function. Trends Cell Biol *21*, 133-140.
3. London, N., and Biggins, S. (2014). Mad1 kinetochore recruitment by Mps1-mediated phosphorylation of Bub1 signals the spindle checkpoint. Genes Dev *28*, 140-152.
4. London, N., Ceto, S., Ranish, J.A., and Biggins, S. (2012). Phosphoregulation of Spc105 by Mps1 and PP1 regulates Bub1 localization to kinetochores. Curr Biol *22*, 900-906.
5. Ji, Z., Gao, H., Jia, L., Li, B., and Yu, H. (2017). A sequential multi-target Mps1 phosphorylation cascade promotes spindle checkpoint signaling. Elife *6*.
6. Faesen, A.C., Thanasoula, M., Maffini, S., Breit, C., Muller, F., van Gerwen, S., Bange, T., and Musacchio, A. (2017). Basis of catalytic assembly of the mitotic checkpoint complex. Nature.
7. Tipton, A.R., Ji, W., Sturt-Gillespie, B., Bekier, M.E., 2nd, Wang, K., Taylor, W.R., and Liu, S.T. (2013). Monopolar spindle 1 (MPS1) kinase promotes production of closed MAD2 (C-MAD2) conformer and assembly of the mitotic checkpoint complex. J Biol Chem *288*, 35149-35158.
8. Hewitt, L., Tighe, A., Santaguida, S., White, A.M., Jones, C.D., Musacchio, A., Green, S., and Taylor, S.S. (2010). Sustained Mps1 activity is required in mitosis to recruit O-Mad2 to the Mad1-C-Mad2 core complex. J Cell Biol *190*, 25-34.
9. Nijenhuis, W., Vallardi, G., Teixeira, A., Kops, G.J., and Saurin, A.T. (2014). Negative feedback at kinetochores underlies a responsive spindle checkpoint signal. Nat Cell Biol *16*, 1257-1264.
10. Saurin, A.T., van der Waal, M.S., Medema, R.H., Lens, S.M., and Kops, G.J. (2011). Aurora B potentiates Mps1 activation to ensure rapid checkpoint establishment at the onset of mitosis. Nat Commun *2*, 316.
11. Pinsky, B.A., Kung, C., Shokat, K.M., and Biggins, S. (2006). The Ipl1-Aurora protein kinase activates the spindle checkpoint by creating unattached kinetochores. Nat Cell Biol *8*, 78-83.
12. Nijenhuis, W., von Castelmur, E., Littler, D., De Marco, V., Tromer, E., Vleugel, M., van Osch, M.H., Snel, B., Perrakis, A., and Kops, G.J. (2013). A TPR domain-containing N-terminal module of MPS1 is required for its kinetochore localization by Aurora B. J Cell Biol *201*, 217-231.
13. Chen, C., Whitney, I.P., Banerjee, A., Sacristan, C., Sekhri, P., Kern, D.M., Fontan, A., Kops, G., Tyson, J.J., Cheeseman, I.M., et al. (2019). Ectopic Activation of the Spindle Assembly Checkpoint Signaling Cascade Reveals Its Biochemical Design. Curr Biol *29*, 104-119 e110.
14. Aravamudhan, P., Goldfarb, A.A., and Joglekar, A.P. (2015). The kinetochore encodes a mechanical switch to disrupt spindle assembly checkpoint signalling. Nat Cell Biol *17*, 868-879.
15. Yuan, I., Leontiou, I., Amin, P., May, K.M., Soper Ni Chafraidh, S., Zlamalova, E., and Hardwick, K.G. (2017). Generation of a Spindle Checkpoint Arrest from Synthetic Signaling Assemblies. Curr Biol *27*, 137-143.
16. Leontiou, I., London, N., May, K.M., Ma, Y., Grzesiak, L., Medina-Pritchard, B., Amin, P., Jeyaprakash, A.A., Biggins, S., and Hardwick, K.G. (2019). The Bub1-TPR Domain Interacts Directly with Mad3 to Generate Robust Spindle Checkpoint Arrest. Curr Biol *29*, 2407-2414 e2407.

17. Di Fiore, B., Davey, Norman E., Hagting, A., Izawa, D., Mansfeld, J., Gibson, Toby J., and Pines, J. (2015). The ABBA Motif Binds APC/C Activators and Is Shared by APC/C Substrates and Regulators. Developmental Cell *32*, 358-372.
18. Morrow, C.J., Tighe, A., Johnson, V.L., Scott, M.I., Ditchfield, C., and Taylor, S.S. (2005). Bub1 and aurora B cooperate to maintain BubR1-mediated inhibition of APC/CCdc20. J Cell Sci *118*, 3639-3652.
19. Ditchfield, C., Johnson, V.L., Tighe, A., Ellston, R., Haworth, C., Johnson, T., Mortlock, A., Keen, N., and Taylor, S.S. (2003). Aurora B couples chromosome alignment with anaphase by targeting BubR1, Mad2, and Cenp-E to kinetochores. J Cell Biol *161*, 267-280.
20. Santaguida, S., Vernieri, C., Villa, F., Ciliberto, A., and Musacchio, A. (2011). Evidence that Aurora B is implicated in spindle checkpoint signalling independently of error correction. EMBO J *30*, 1508-1519.
21. Vanoosthuyse, V., and Hardwick, K.G. (2009). A novel protein phosphatase 1-dependent spindle checkpoint silencing mechanism. Curr Biol *19*, 1176-1181.
22. Hauf, S., Cole, R.W., LaTerra, S., Zimmer, C., Schnapp, G., Walter, R., Heckel, A., van Meel, J., Rieder, C.L., and Peters, J.M. (2003). The small molecule Hesperadin reveals a role for Aurora B in correcting kinetochore-microtubule attachment and in maintaining the spindle assembly checkpoint. J Cell Biol *161*, 281-294.
23. Vader, G., Cruijsen, C.W., van Harn, T., Vromans, M.J., Medema, R.H., and Lens, S.M. (2007). The chromosomal passenger complex controls spindle checkpoint function independent from its role in correcting microtubule kinetochore interactions. Mol Biol Cell *18*, 4553-4564.
24. King, E.M., Rachidi, N., Morrice, N., Hardwick, K.G., and Stark, M.J. (2007). Ipl1p-dependent phosphorylation of Mad3p is required for the spindle checkpoint response to lack of tension at kinetochores. Genes Dev *21*, 1163-1168.
25. Haruki, H., Nishikawa, J., and Laemmli, U.K. (2008). The anchor-away technique: rapid, conditional establishment of yeast mutant phenotypes. Mol Cell *31*, 925-932.
26. Kim, T., Moyle, M.W., Lara-Gonzalez, P., De Groot, C., Oegema, K., and Desai, A. (2015). Kinetochore-localized BUB-1/BUB-3 complex promotes anaphase onset in C. elegans. J Cell Biol *209*, 507-517.
27. Weir, J.R., Faesen, A.C., Klare, K., Petrovic, A., Basilico, F., Fischbock, J., Pentakota, S., Keller, J., Pesenti, M.E., Pan, D., et al. (2016). Insights from biochemical reconstitution into the architecture of human kinetochores. Nature *537*, 249-253.
28. Fischer, E.S., Yu, C.W.H., Bellini, D., McLaughlin, S.H., Orr, C.M., Wagner, A., Freund, S.M.V., and Barford, D. (2021). Molecular mechanism of Mad1 kinetochore targeting by phosphorylated Bub1. EMBO Rep, e52242.
29. Vleugel, M., Hoek, T.A., Tromer, E., Sliedrecht, T., Groenewold, V., Omerzu, M., and Kops, G.J. (2015). Dissecting the roles of human BUB1 in the spindle assembly checkpoint. J Cell Sci *128*, 2975-2982.
30. Roy, B., Han, S.J.Y., Fontan, A.N., and Joglekar, A.P. (2020). The copy-number and varied strength of MELT motifs in Spc105 balance the strength and responsiveness of the Spindle Assembly Checkpoint. Elife *9*.
31. Primorac, I., Weir, J.R., Chiroli, E., Gross, F., Hoffmann, I., van Gerwen, S., Ciliberto, A., and Musacchio, A. (2013). Bub3 reads phosphorylated MELT repeats to promote spindle assembly checkpoint signaling. Elife *2*, e01030.
32. Piano, V., Alex, A., Stege, P., Maffini, S., Stoppiello, G.A., Huis In 't Veld, P.J., Vetter, I.R., and Musacchio, A. (2021). CDC20 assists its catalytic incorporation in the mitotic checkpoint complex. Science *371*, 67-71.

33. Lara-Gonzalez, P., Kim, T., Oegema, K., Corbett, K., and Desai, A. (2021). A tripartite mechanism catalyzes Mad2-Cdc20 assembly at unattached kinetochores. Science *371*, 64-67.
34. Overlack, K., Primorac, I., Vleugel, M., Krenn, V., Maffini, S., Hoffmann, I., Kops, G.J., and Musacchio, A. (2015). A molecular basis for the differential roles of Bub1 and BubR1 in the spindle assembly checkpoint. Elife *4*, e05269.
35. Zhang, G., Mendez, B.L., Sedgwick, G.G., and Nilsson, J. (2016). Two functionally distinct kinetochore pools of BubR1 ensure accurate chromosome segregation. Nat Commun *7*, 12256.
36. Tromer, E., Bade, D., Snel, B., and Kops, G.J. (2016). Phylogenomics-guided discovery of a novel conserved cassette of short linear motifs in BubR1 essential for the spindle checkpoint. Open Biol *6*.
37. Rosenberg, J.S., Cross, F.R., and Funabiki, H. (2011). KNL1/Spc105 recruits PP1 to silence the spindle assembly checkpoint. Curr Biol *21*, 942-947.
38. Garcia-Rodriguez, L.J., Kasciukovic, T., Denninger, V., and Tanaka, T.U. (2019). Aurora B-INCENP Localization at Centromeres/Inner Kinetochores Is Required for Chromosome Bi-orientation in Budding Yeast. Curr Biol *29*, 1536-1544 e1534.
39. Nakajima, Y., Cormier, A., Tyers, R.G., Pigula, A., Peng, Y., Drubin, D.G., and Barnes, G. (2011). Ipl1/Aurora-dependent phosphorylation of Sli15/INCENP regulates CPC-spindle interaction to ensure proper microtubule dynamics. J Cell Biol *194*, 137-153.
40. Larsen, N.A., Al-Bassam, J., Wei, R.R., and Harrison, S.C. (2007). Structural analysis of Bub3 interactions in the mitotic spindle checkpoint. Proc Natl Acad Sci USA *104*, 1201-1206.
41. Maure, J.F., Kitamura, E., and Tanaka, T.U. (2007). Mps1 kinase promotes sister-kinetochore bi-orientation by a tension-dependent mechanism. Curr Biol *17*, 2175-2182.
42. Biggins, S., and Murray, A.W. (2001). The budding yeast protein kinase Ipl1/Aurora allows the absence of tension to activate the spindle checkpoint. Genes Dev *15*, 3118-3129.
43. Roy, B., Verma, V., Sim, J., Fontan, A., and Joglekar, A.P. (2019). Delineating the contribution of Spc105-bound PP1 to spindle checkpoint silencing and kinetochore microtubule attachment regulation. J Cell Biol.
44. Ballister, E.R., Riegman, M., and Lampson, M.A. (2014). Recruitment of Mad1 to metaphase kinetochores is sufficient to reactivate the mitotic checkpoint. J Cell Biol *204*, 901-908.
45. Maldonado, M., and Kapoor, T.M. (2011). Constitutive Mad1 targeting to kinetochores uncouples checkpoint signalling from chromosome biorientation. Nat Cell Biol *13*, 475-482.
46. Kuijt, T.E., Omerzu, M., Saurin, A.T., and Kops, G.J. (2014). Conditional targeting of MAD1 to kinetochores is sufficient to reactivate the spindle assembly checkpoint in metaphase. Chromosoma *123*, 471-480.
47. Kruse, T., Larsen, M.S.Y., Sedgwick, G.G., Sigurdsson, J.O., Streicher, W., Olsen, J.V., and Nilsson, J. (2014). A direct role of Mad1 in the spindle assembly checkpoint beyond Mad2 kinetochore recruitment. EMBO reports *15*, 282-290.
48. Vleugel, M., Omerzu, M., Groenewold, V., Hadders, M.A., Lens, S.M., and Kops, G.J. (2015). Sequential multisite phospho-regulation of KNL1-BUB3 interfaces at mitotic kinetochores. Mol Cell *57*, 824-835.
49. Sessa, F., Mapelli, M., Ciferri, C., Tarricone, C., Areces, L.B., Schneider, T.R., Stukenberg, P.T., and Musacchio, A. (2005). Mechanism of Aurora B activation by INCENP and inhibition by hesperadin. Mol Cell *18*, 379-391.
50. Lee, S., Thebault, P., Freschi, L., Beaufils, S., Blundell, T.L., Landry, C.R., Bolanos-Garcia, V.M., and Elowe, S. (2012). Characterization of spindle checkpoint kinase Mps1

reveals domain with functional and structural similarities to tetratricopeptide repeat motifs of Bub1 and BubR1 checkpoint kinases. J Biol Chem *287*, 5988-6001.

51. Mora-Santos, M.D., Hervas-Aguilar, A., Sewart, K., Lancaster, T.C., Meadows, J.C., and Millar, J.B. (2016). Bub3-Bub1 Binding to Spc7/KNL1 Toggles the Spindle Checkpoint Switch by Licensing the Interaction of Bub1 with Mad1-Mad2. Curr Biol *26*, 2642-2650.
52. Ishihara, H., Martin, B.L., Brautigan, D.L., Karaki, H., Ozaki, H., Kato, Y., Fusetani, N., Watabe, S., Hashimoto, K., Uemura, D., et al. (1989). Calyculin A and okadaic acid: inhibitors of protein phosphatase activity. Biochem. Biophys. Res. Commun. *159*, 871-877.
53. Qian, J., Garcia-Gimeno, M.A., Beullens, M., Manzione, M.G., Van der Hoeven, G., Igual, J.C., Heredia, M., Sanz, P., Gelens, L., and Bollen, M. (2017). An Attachment-Independent Biochemical Timer of the Spindle Assembly Checkpoint. Mol Cell *68*, 715-730 e715.
54. Etemad, B., Kuijt, T.E., and Kops, G.J. (2015). Kinetochore-microtubule attachment is sufficient to satisfy the human spindle assembly checkpoint. Nat Commun *6*, 8987.
55. Tauchman, E.C., Boehm, F.J., and DeLuca, J.G. (2015). Stable kinetochore-microtubule attachment is sufficient to silence the spindle assembly checkpoint in human cells. Nat Commun *6*, 10036.
56. Kuhn, J., and Dumont, S. (2019). Mammalian kinetochores count attached microtubules in a sensitive and switch-like manner. J Cell Biol *218*, 3583-3596.
57. Dick, A.E., and Gerlich, D.W. (2013). Kinetic framework of spindle assembly checkpoint signalling. Nat Cell Biol *15*, 1370-1377.
58. Kops, G., and Gassmann, R. (2020). Crowning the Kinetochore: The Fibrous Corona in Chromosome Segregation. Trends Cell Biol *30*, 653-667.
59. Aravamudhan, P., Chen, R., Roy, B., Sim, J., and Joglekar, A.P. (2016). Dual mechanisms regulate the recruitment of spindle assembly checkpoint proteins to the budding yeast kinetochore. Mol Biol Cell *27*, 3405-3417.
60. Jürg Bähler, Jian-Qiu Wu, Mark S. Longtine, Nirav G. Shah, Amos Mckenzie III, Alexander B. Steever, Achim Wach, Peter Philippsen, and Pringle, J.R. (1998). Heterologous modules for efficient and versatile PCR-based gene targeting in Schizosaccharomyces pombe. YEAST *14*, 943-951.
61. Scott, R.J., Lusk, C.P., Dilworth, D.J., Aitchison, J.D., and Wozniak, R.W. (2005). Interactions between Mad1p and the nuclear transport machinery in the yeast Saccharomyces cerevisiae. Mol Biol Cell *16*, 4362-4374.
62. Kemmler, S., Stach, M., Knapp, M., Ortiz, J., Pfannstiel, J., Ruppert, T., and Lechner, J. (2009). Mimicking Ndc80 phosphorylation triggers spindle assembly checkpoint signalling. EMBO J *28*, 1099-1110.
63. Gillett, E.S., Espelin, C.W., and Sorger, P.K. (2004). Spindle checkpoint proteins and chromosome–microtubule attachment in budding yeast. The Journal of Cell Biology *164*, 535-546.
64. Aravamudhan, P., Felzer-Kim, I., Gurunathan, K., and Joglekar, A.P. (2014). Assembling the protein architecture of the budding yeast kinetochore-microtubule attachment using FRET. Curr Biol *24*, 1437-1446.
65. Joglekar, A., Chen, R., and Lawrimore, J. (2013). A Sensitized Emission Based Calibration of FRET Efficiency for Probing the Architecture of Macromolecular Machines. Cell Mol Bioeng *6*, 369-382.
66. Khandelia, P., Yap, K., and Makeyev, E.V. (2011). Streamlined platform for short hairpin RNA interference and transgenesis in cultured mammalian cells. Proc Natl Acad Sci USA *108*, 12799-12804.
67. Collin, P., Nashchekina, O., Walker, R., and Pines, J. (2013). The spindle assembly checkpoint works like a rheostat rather than a toggle switch. Nat Cell Biol *15*, 1378-1385.

68. Gupta, A., Evans, R.K., Koch, L.B., Littleton, A.J., and Biggins, S. (2018). Purification of kinetochores from the budding yeast Saccharomyces cerevisiae. Methods in cell biology *144*, 349-370.

Figure 1

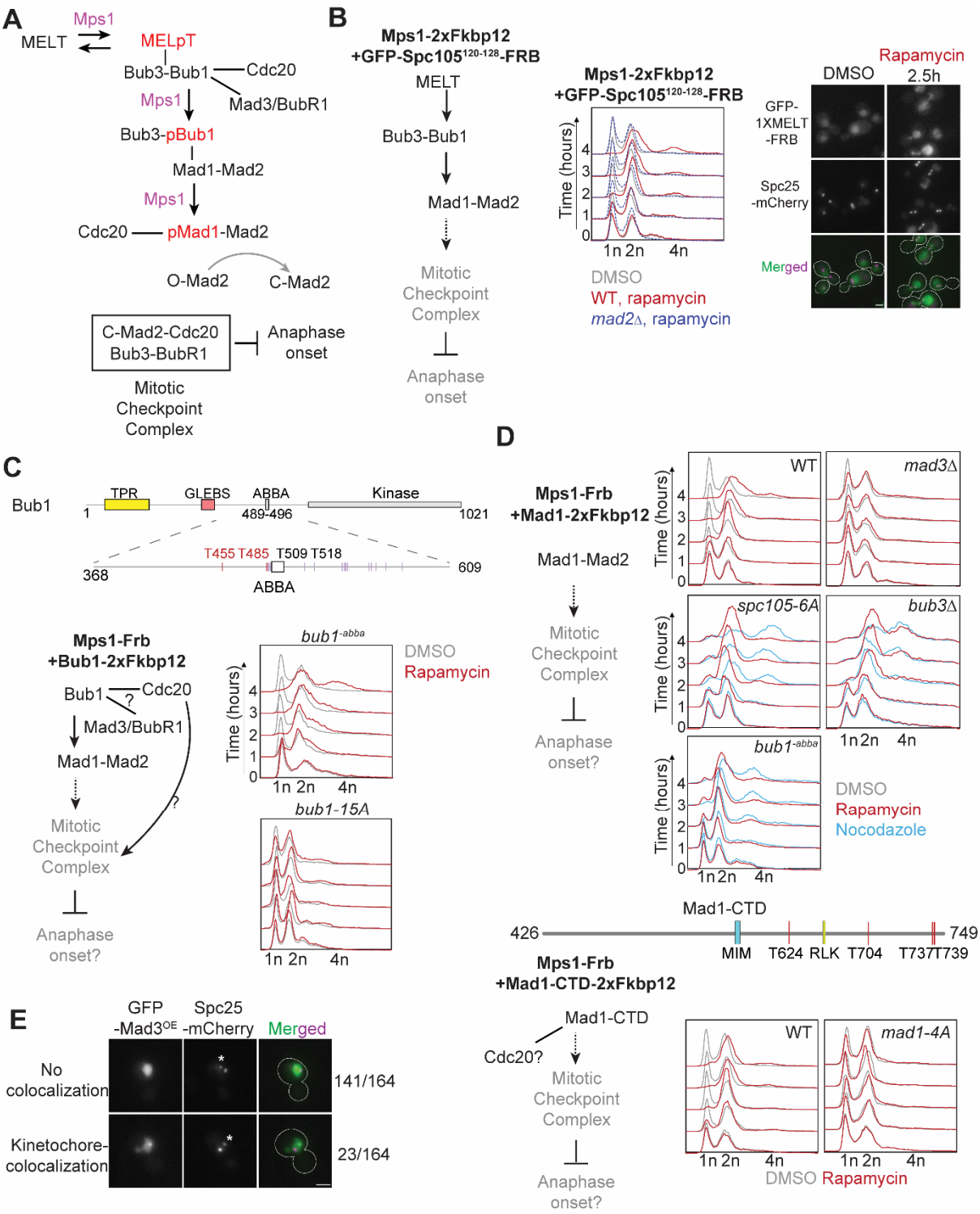
A
Mps1
MELT
MELpT
Bub3-Bub1
Cdc20
Mps1
Mad3/BubR1
Bub3-pBub1
Mad1-Mad2
Mps1
Cdc20
pMad1-Mad2
O-Mad2
C-Mad2
C-Mad2-Cdc20
Bub3-BubR1
Anaphase onset
Mitotic Checkpoint Complex
B
Mps1-2xFkbp12
+GFP-Spc105120-128-FRB
MELT
Bub3-Bub1
Mad1-Mad2
Mitotic Checkpoint Complex
Anaphase onset
Mps1-2xFkbp12
+GFP-Spc105120-128-FRB
Time (hours)
1n 2n 4n
DMSO
WT, rapamycin
mad2Δ, rapamycin
DMSO
Rapamycin 2.5h
GFP-1XMELT-FRB
Spc25-mCherry
Merged
C
Bub1
TPR
GLEBS
ABBA
Kinase
1
489-496
1021
T455 T485 T509 T518
368
609
ABBA
Mps1-Frb
+Bub1-2xFkbp12
Bub1
Cdc20
Mad3/BubR1
Mad1-Mad2
Mitotic Checkpoint Complex
Anaphase onset?
bub1-abba
bub1-15A
DMSO
Rapamycin
Time (hours)
1n 2n 4n
D
Mps1-Frb
+Mad1-2xFkbp12
Mad1-Mad2
Mitotic Checkpoint Complex
Anaphase onset?
WT
mad3Δ
spc105-6A
bub3Δ
bub1-abba
Time (hours)
1n 2n 4n
DMSO
Rapamycin
Nocodazole
Mad1-CTD
426
749
MIM
T624
RLK
T704
T737T739
Mps1-Frb
+Mad1-CTD-2xFkbp12
Mad1-CTD
Cdc20?
Mitotic Checkpoint Complex
Anaphase onset?
WT
mad1-4A
1n 2n 4n
DMSO
Rapamycin
E
GFP-Mad3OE
Spc25-mCherry
Merged
No colocalization
141/164
Kinetochore-colocalization
23/164

1143 **Figure 2**

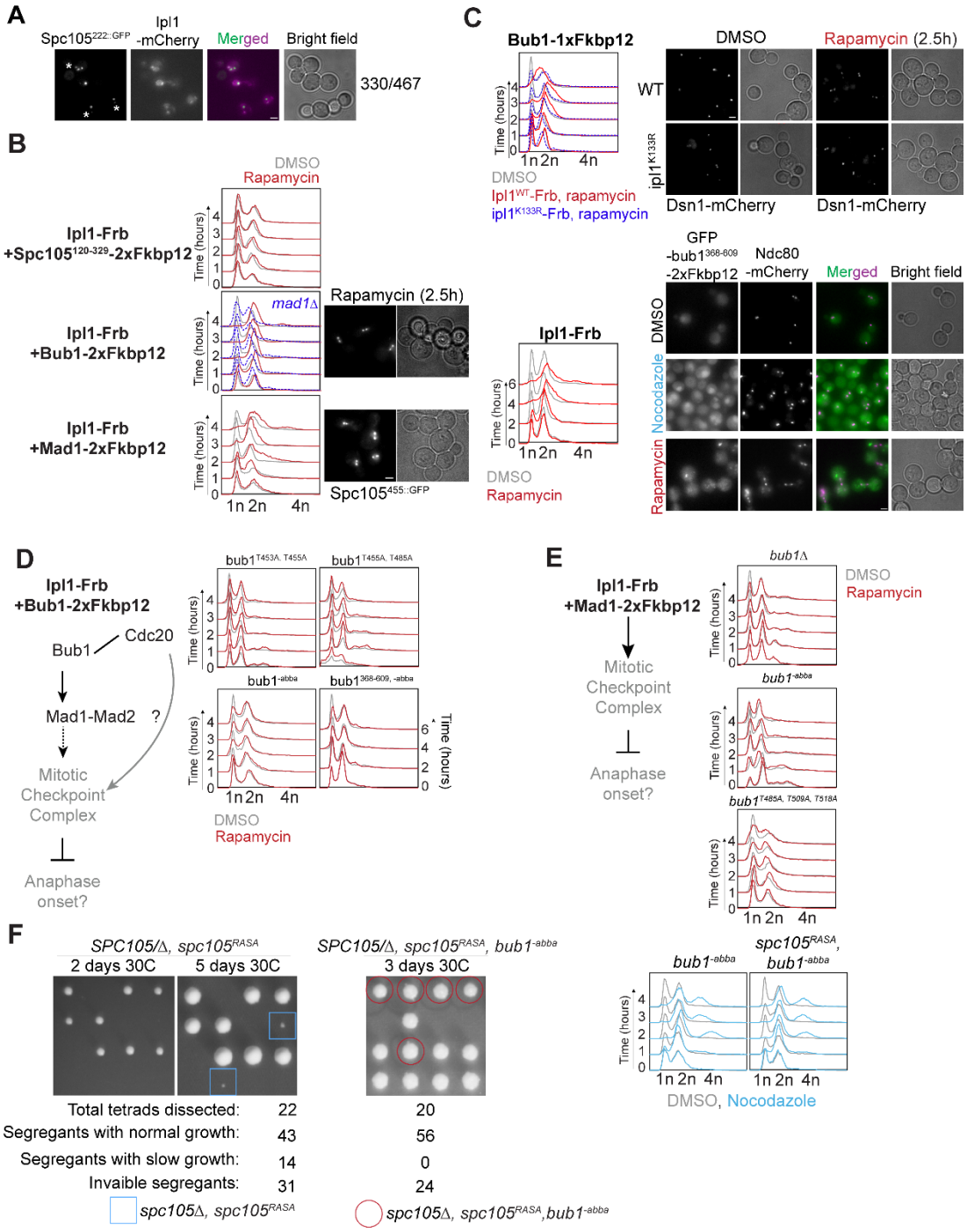

1144

1145

Figure 3

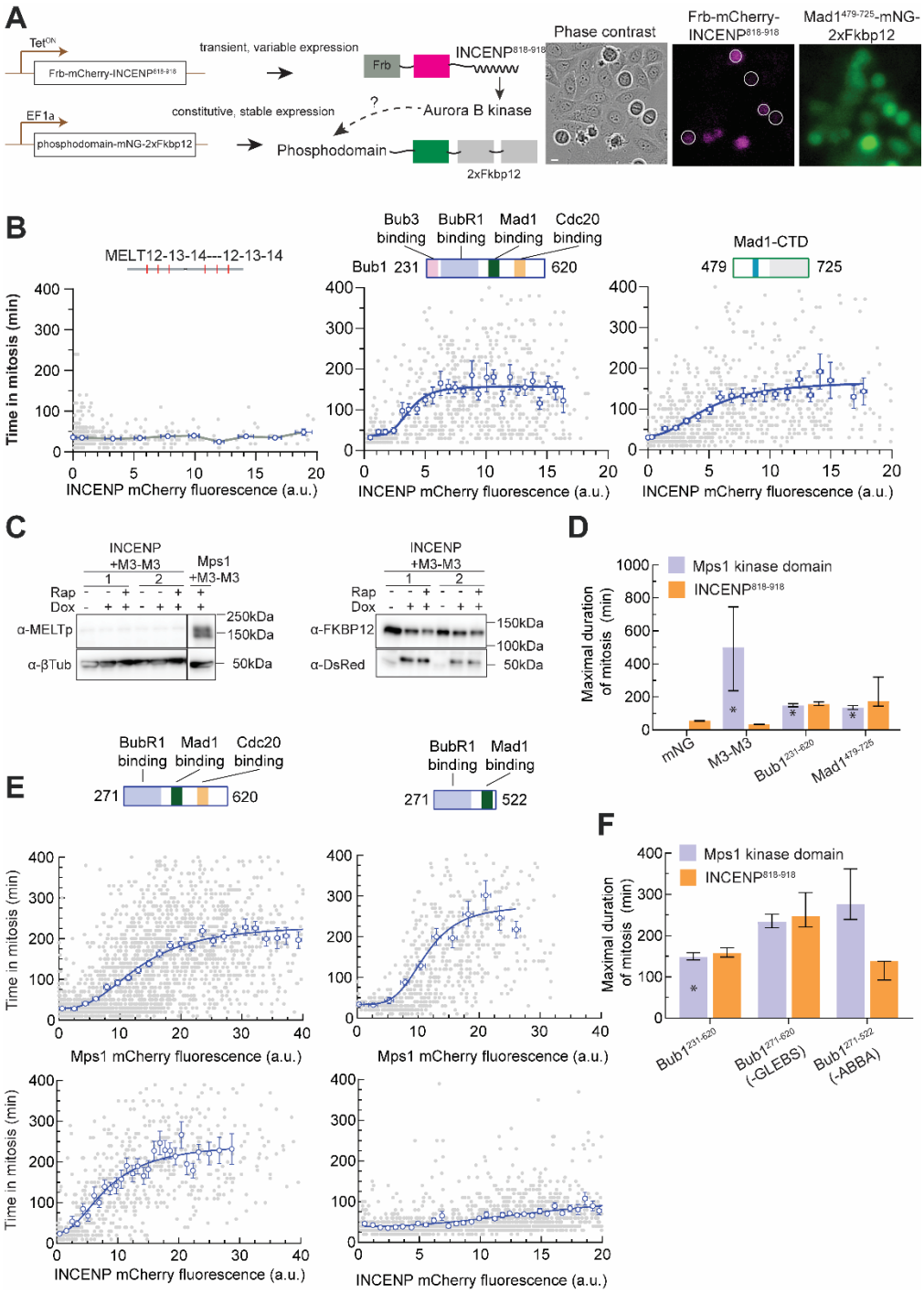
A
Tet^ON
Frb-mCherry-INCENP818-918
transient, variable expression
Frb
INCENP818-918
Aurora B kinase
EF1a
phosphodomain-mNG-2xFkbp12
constitutive, stable expression
Phosphodomain
2xFkbp12
Phase contrast
Frb-mCherry-INCENP818-918
Mad1479-725-mNG-2xFkbp12
B
MELT12-13-14---12-13-14
Bub3 binding
BubR1 binding
Mad1 binding
Cdc20 binding
Bub1 231
620
Mad1-CTD
479
725
Time in mitosis (min)
INCENP mCherry fluorescence (a.u.)
C
INCENP +M3-M3
Mps1 +M3-M3
Rap
Dox
α-MELTp
α-βTub
250kDa
150kDa
50kDa
α-FKBP12
α-DsRed
100kDa
D
Mps1 kinase domain
INCENP818-918
Maximal duration of mitosis (min)
mNG
M3-M3
Bub1231-620
Mad1479-725
E
271
620
522
Mps1 mCherry fluorescence (a.u.)
F
Bub1231-620
Bub1271-620 (-GLEBS)
Bub1271-522 (-ABBA)

1149 **Figure 4**

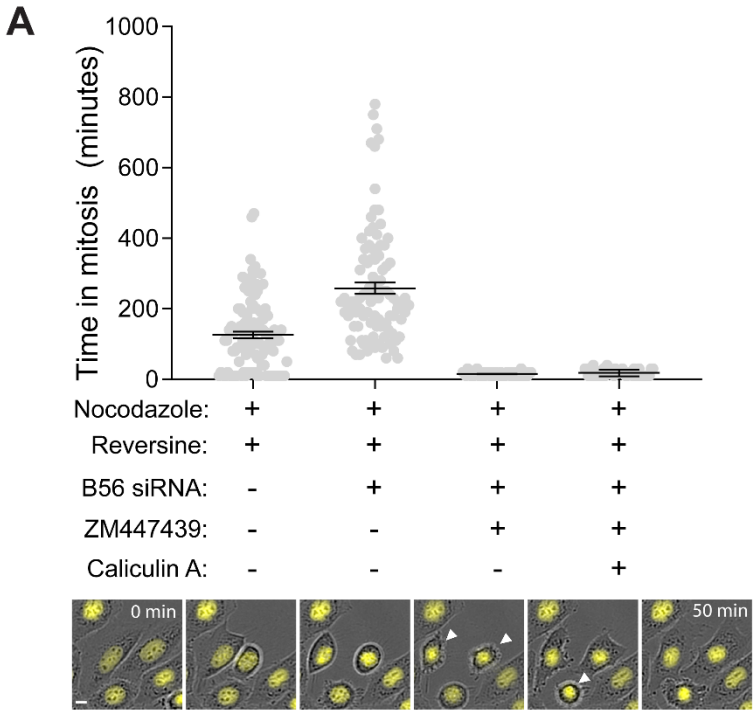

B

Checkpoint proteins used in eSAC experiments	Cassettes used in eSAC experiments	Mps1 mediated mitotic arrest	Ipl1 mediated mitotic arrest
Spc105	phosphodomain	Yes	No
Bub1	WT	Yes	Yes
	-ABBA	Yes	No
	-Mad1	No	No
Mad1	WT	Yes	Yes
	-Cdc20	No	Not done

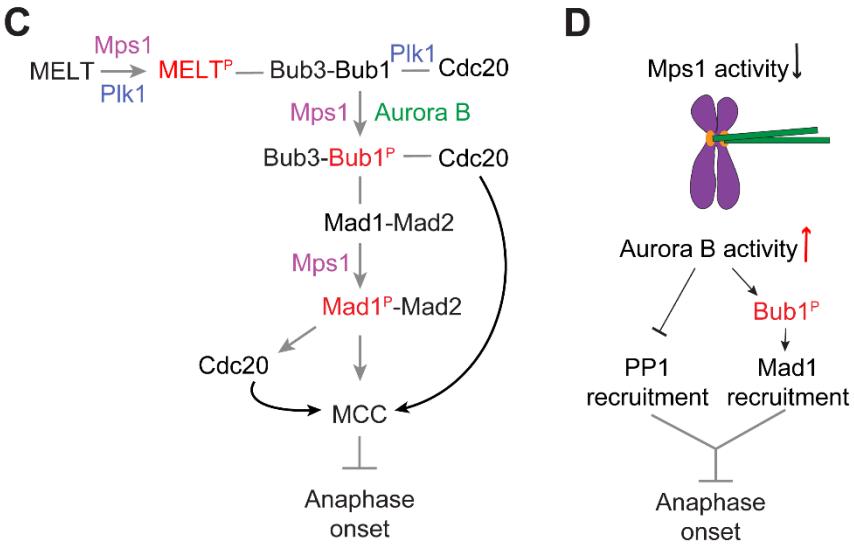

1150

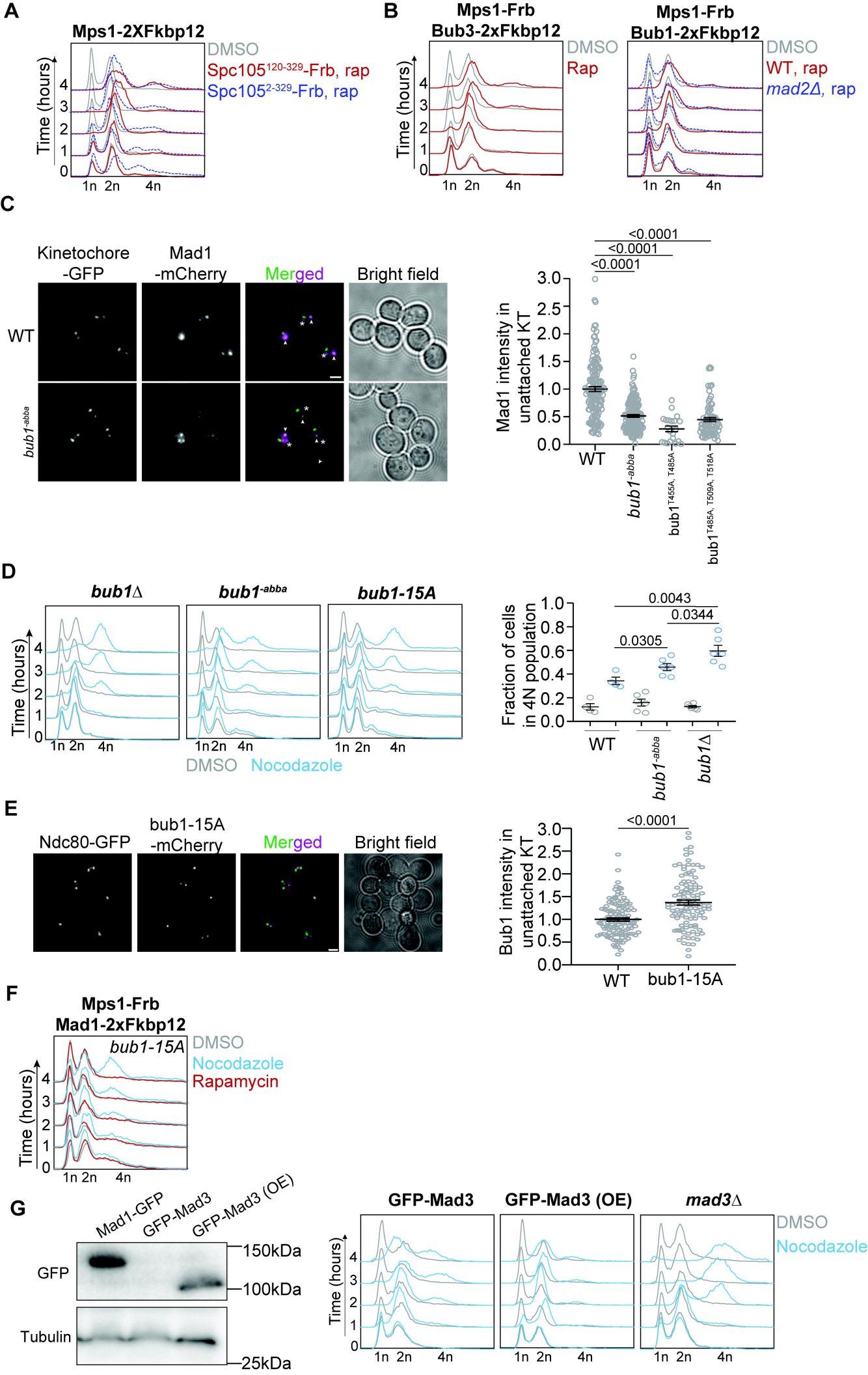
A
Mps1-2XFkbp12
DMSO
Spc105120-329-Frb, rap
Spc1052-329-Frb, rap
Time (hours)
1n 2n 4n
B
Mps1-Frb
Bub3-2xFkbp12
DMSO
Rap
Mps1-Frb
Bub1-2xFkbp12
DMSO
WT, rap
mad2Δ, rap
C
Kinetochore -GFP
Mad1 -mCherry
Merged
Bright field
WT
bub1-abba
Mad1 intensity in unattached KT
<0.0001
<0.0001
<0.0001
WT
bub1-abba
bub1T455A, T485A
bub1T485A, T509A, T518A
D
bub1Δ
bub1-abba
bub1-15A
DMSO Nocodazole
Fraction of cells in 4N population
0.0043
0.0344
0.0305
WT
bub1-abba
bub1Δ
E
Ndc80-GFP
bub1-15A -mCherry
Merged
Bright field
Bub1 intensity in unattached KT
<0.0001
WT
bub1-15A
F
Mps1-Frb
Mad1-2xFkbp12
bub1-15A
DMSO
Nocodazole
Rapamycin
G
Mad1-GFP
GFP-Mad3
GFP-Mad3 (OE)
GFP
Tubulin
150kDa
100kDa
25kDa
GFP-Mad3
GFP-Mad3 (OE)
mad3Δ
DMSO
Nocodazole

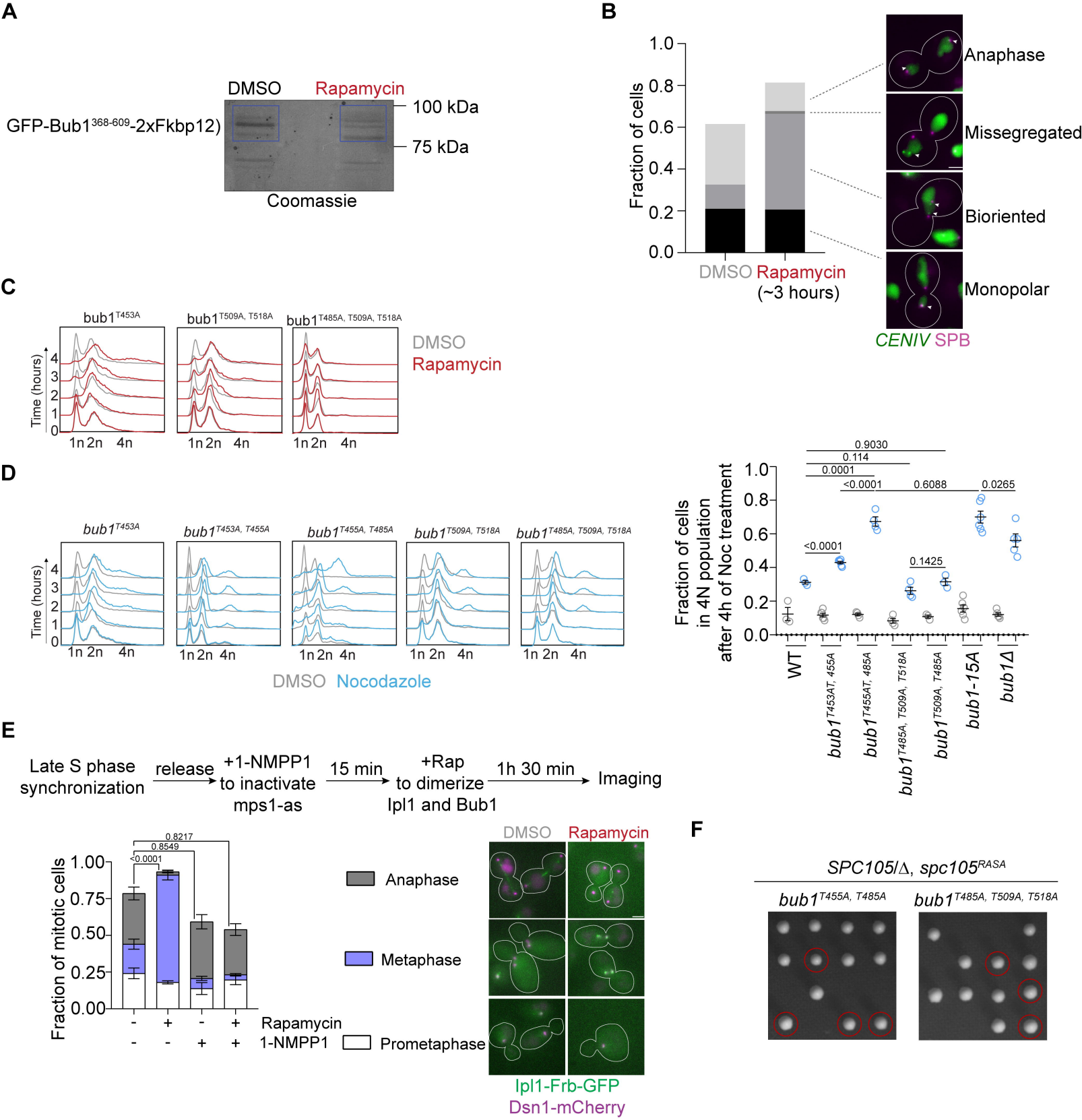

G

Bub1 mutant	Kinase	Mitotic arrest in nocodazole?	Mitotic arrest in rapamycin?
T453A	Mps1	yes	yes
	Ipl1	yes	yes
T453A, T455A	Mps1	yes	yes
	Ipl1	yes	**No**
T455A, T485A	Mps1	yes	yes
	Ipl1	**No**	**No**
T485A, T509A, T518A	Mps1	yes	yes
	Ipl1	yes	**No**
T509A, T518A	Mps1	yes	yes
	Ipl1	yes	yes
15A	Mps1	No	No
	Ipl1	No	No
-abba	Mps1	yes	yes
	Ipl1	yes	**No**

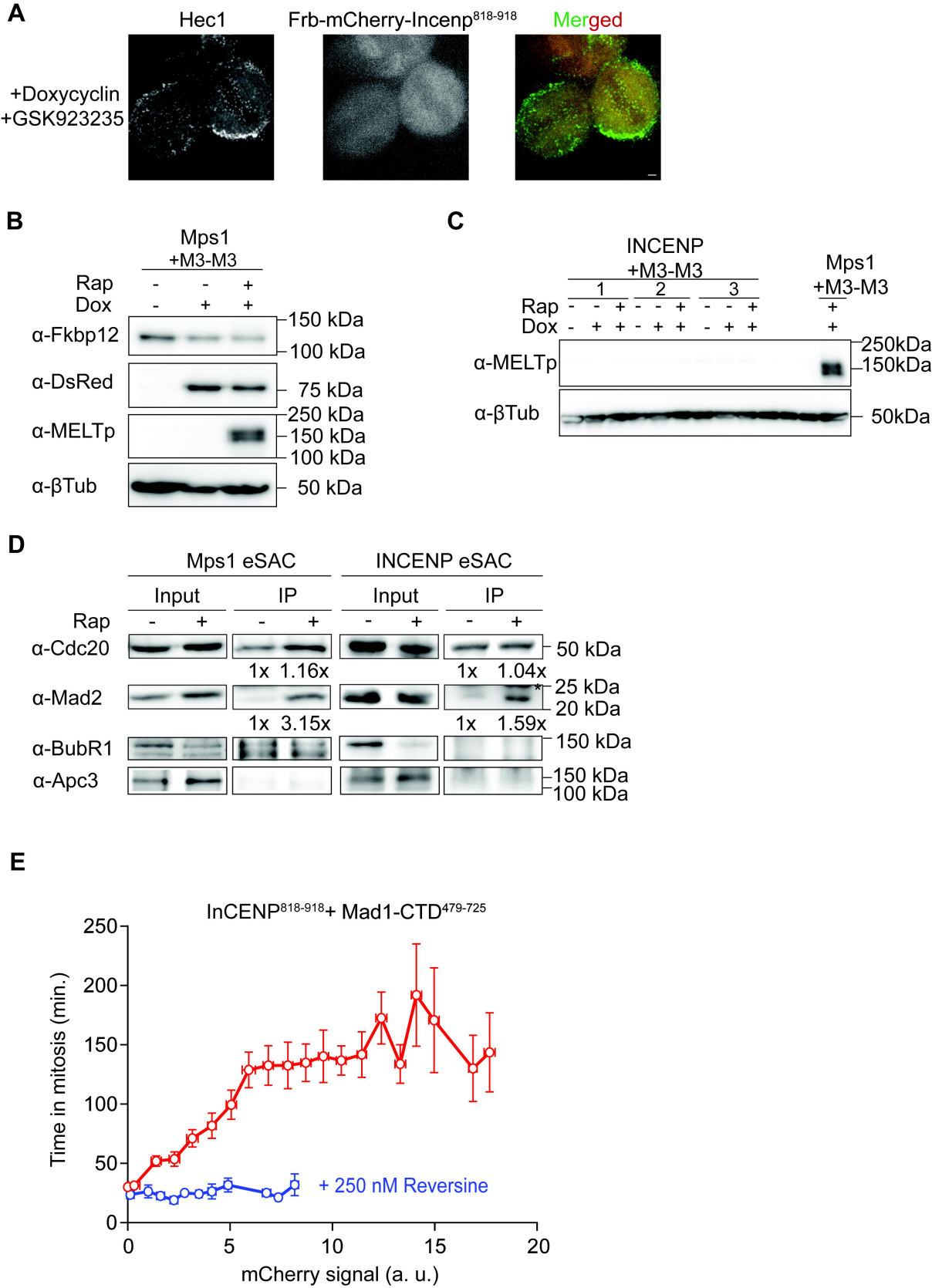
A
Hec1
Frb-mCherry-Incenp818-918
Merged
+Doxycyclin
+GSK923235
B
Mps1
+M3-M3
Rap
Dox
α-Fkbp12
α-DsRed
α-MELTp
α-βTub
150 kDa
100 kDa
75 kDa
250 kDa
150 kDa
100 kDa
50 kDa
C
INCENP
+M3-M3
1
2
3
Mps1
+M3-M3
Rap
Dox
α-MELTp
α-βTub
250kDa
150kDa
50kDa
D
Mps1 eSAC
INCENP eSAC
Input
IP
Input
IP
Rap
α-Cdc20
α-Mad2
α-BubR1
α-Apc3
1x 1.16x
1x 1.04x
1x 3.15x
1x 1.59x
50 kDa
25 kDa
20 kDa
150 kDa
150 kDa
100 kDa
E
InCENP818-918+ Mad1-CTD479-725
Time in mitosis (min.)
mCherry signal (a. u.)
+ 250 nM Reversine
0
50
100
150
200
250
0
5
10
15
20